

Standardizing Dainotti-correlated gamma-ray bursts, and using them with standardized Amati-correlated gamma-ray bursts to constrain cosmological model parameters

Shulei Cao,^{ID1*} Narayan Khadka,^{ID1†} Bharat Ratra^{ID1‡}

¹*Department of Physics, Kansas State University, 116 Cardwell Hall, Manhattan, KS 66502, USA*

Accepted XXX. Received YYY; in original form ZZZ

ABSTRACT

We show that each of the three Dainotti-correlated gamma-ray burst (GRB) data sets recently compiled by Wang et al. and Hu et al., that together probe the redshift range $0.35 \leq z \leq 5.91$, obey cosmological-model-independent Dainotti correlations and so are standardizable. We use these GRB data in conjunction with the best currently-available Amati-correlated GRB data, that probe $0.3399 \leq z \leq 8.2$, to constrain cosmological model parameters. The resulting cosmological constraints are weak, providing lower limits on the non-relativistic matter density parameter, mildly favoring non-zero spatial curvature, and largely consistent with currently accelerated cosmological expansion as well as with constraints determined from better-established data.

Key words: cosmological parameters – dark energy – cosmology: observations – gamma-ray bursts

1 INTRODUCTION

The observed currently accelerated cosmological expansion indicates that — if general relativity provides an accurate description of gravitation on cosmological scales — dark energy must contribute significantly to the current cosmological energy budget. The simpler spatially-flat Λ CDM model (Peebles 1984) is consistent with this and other observations. Fits of this model to most better-established cosmological data suggest that a time-independent cosmological constant (Λ) provides $\sim 70\%$ of the current cosmological energy budget, non-relativistic cold dark matter (CDM) provides $\sim 25\%$, and non-relativistic baryonic matter provides most of the remaining $\sim 5\%$ (see, e.g. Farooq et al. 2017; Scolnic et al. 2018; Planck Collaboration 2020; eBOSS Collaboration 2021). While the spatially-flat Λ CDM model is consistent with most observations (see, e.g. Di Valentino et al. 2021b; Perivolaropoulos & Skara 2021), observational data do not strongly rule out a little spatial curvature or dynamical dark energy. In this paper, in addition to the spatially-flat Λ CDM model, we also study spatially non-flat and dynamical dark energy models.

Observational astronomy now provides many measurements that can be used to test cosmological models. Largely,

these data are either at low or at high redshift. So cosmological models are mostly tested at low and high redshifts, remaining poorly tested in the intermediate redshift regime. The highest redshift of the better-established low-redshift data, ~ 2.3 , is reached through baryon acoustic oscillation (BAO) observations; the high redshift region, $z \sim 1100$, is probed by better-established cosmic microwave background anisotropy data. Fits of these better-established data to cosmological models provide mostly mutually consistent results. However, for a better understanding of our Universe, it is necessary to also test cosmological models in the intermediate redshift range of $2.3 \lesssim z \lesssim 1100$. Some progress has been achieved: methods that test cosmological models in the intermediate redshift region include the use of H II starburst galaxy measurements which reach to $z \sim 2.4$ (Mania & Ratra 2012; Chávez et al. 2014; González-Morán et al. 2019, 2021; Cao et al. 2020, 2021a,b; Johnson et al. 2021), quasar angular size measurements which reach to ~ 2.7 (Cao et al. 2017; Ryan et al. 2019; Cao et al. 2020, 2021b; Zheng et al. 2021; Lian et al. 2021), and quasar flux measurements which reach to ~ 7.5 (Risaliti & Lusso 2015, 2019; Khadka & Ratra 2020a,b, 2021a,b; Yang et al. 2020; Lusso et al. 2020; Zhao & Xia 2021; Li et al. 2021; Lian et al. 2021; Rezaei et al. 2021; Luongo et al. 2021).¹

* E-mail: shulei@phys.ksu.edu

† E-mail: nkhadka@phys.ksu.edu

‡ E-mail: ratra@phys.ksu.edu

Gamma-ray burst (GRB) measurements are another high redshift probe and reach to $z \sim 8.2$ (Amati et al. 2008, 2019; Salvaterra et al. 2009; Tanvir et al. 2009; Samushia & Ratra 2010; Cardone et al. 2010; Dainotti et al. 2013a; Wang et al. 2015, 2016; Dainotti & Del Vecchio 2017; Fana Dirirsa et al. 2019; Khadka & Ratra 2020c; Demianski et al. 2021; Khadka et al. 2021b; Luongo et al. 2021; Luongo & Muccino 2021). While there are quite a few Amati correlation long GRBs that have been used to constrain cosmological parameters, currently only a smaller fraction of 118 such GRBs (hereafter A118) that cover the redshift range $0.3399 \leq z \leq 8.2$ (Khadka & Ratra 2020c; Khadka et al. 2021a) are reliable enough to be used to constrain cosmological parameters. To date, this is the lower- z data set used to constrain cosmological parameters that spans the widest range of redshifts. These A118 data provide cosmological constraints which are consistent with those obtained from the better-established cosmological probes but the GRB constraints are significantly less restrictive. To obtain tighter cosmological constraints using GRB data, we need to make use of more GRBs.

Recently Wang et al. (2021) and Hu et al. (2021) have compiled smaller GRB data sets that together probe the redshift range $0.35 \leq z \leq 5.91$. These are GRBs whose plateau phase luminosity L_0 and spin-down characteristic time t_b are correlated through the Dainotti ($L_0 - t_b$) correlation (Dainotti et al. 2013b, 2017). This correlation between L_0 and t_b allows one to use these GRBs for cosmological purposes. These GRBs can be classified in two categories depending on whether the plateau phase is dominated by magnetic dipole (MD) radiation or gravitational wave (GW) emission (Wang et al. 2021; Hu et al. 2021). In this paper we use long and short GRBs whose plateau phase is dominated by MD radiation (hereafter MD-LGRBs and MD-SGRBs) and long GRBs whose plateau phase is dominated by GW emission (hereafter GW-LGRBs). All three sets of GRBs obey the Dainotti correlation but each set can have different correlation parameters. We use the three individual GRB data sets, as well as some combinations of them, to constrain cosmological model parameters and Dainotti correlation parameters simultaneously.² We find that these GRBs are standardizable, as was assumed in Wang et al. (2021) and Hu et al. (2021). However, cosmological constraints obtained from these Dainotti correlation GRB data sets are very weak.

When we combine the MD-LGRB or GW-LGRB data sets with the 115 non-overlapping Amati correlation GRBs from the A118 data set, they slightly tighten the constraints from the 115 Amati correlation GRBs, but not significantly so. Each of the individual Amati or Dainotti correlation GRB data sets, as well as combinations of these GRB data sets, mostly provide only lower limits on the current value of the non-relativistic matter energy density

to derive only lower- z cosmological constraints (Khadka & Ratra 2021a,b).

² The advantage of fitting cosmological and GRB correlation parameters simultaneously is that the fitting process is free from the circularity problem. More specifically, this procedure allows us to determine whether the GRB correlation parameters depend on the assumed cosmological model and so determine whether the GRBs are standardizable.

parameter Ω_{m0} and the resulting cosmological parameter constraints are mostly consistent with those obtained from better-established cosmological data.

In this paper, we use a combination of Hubble parameter ($H(z)$) and BAO data, $H(z) + \text{BAO}$, results as a proxy for better-established data results, to compare with our GRB data results. Qualitatively, results from the individual GRB data sets, as well as those from combinations of GRB data sets, are consistent with those from the $H(z) + \text{BAO}$ data which favor $\Omega_{m0} \sim 0.3$, but there are a few combinations of GRB data sets with constraints on Ω_{m0} being more than 2σ away from 0.3 in the ΛCDM models.

This paper is structured as follows. In Sec. 2 we summarize the cosmological models we use. In Sec. 3 we describe the data sets we analyze. In Sec. 4 we summarize our analyses techniques. In Sec. 5 we present our results. We conclude in Sec. 6.

2 COSMOLOGICAL MODELS

In this paper we derive cosmological parameter constraints in six different general-relativity cosmological dark energy models. Three of them assume spatially-flat geometry while the other three allow non-flat spatial geometry.³ These models are used to predict the luminosity distance for a GRB at a given redshift. For this purpose the fundamental quantity is the expansion rate of the Universe, or the Hubble parameter, $H(z)$, a function of cosmological parameters and redshift.

The Hubble parameter in all six models we use can be written as

$$H(z) = H_0 \sqrt{\Omega_{m0}(1+z)^3 + \Omega_{k0}(1+z)^2 + \Omega_{\text{DE}}(z)}, \quad (1)$$

where H_0 is the Hubble constant and Ω_{k0} is the current value of the spatial curvature energy density parameter. In analyses of the $H(z) + \text{BAO}$ data set we express Ω_{m0} in terms of the current value of the baryonic matter energy density parameter (Ω_b) and the current value of the cold dark matter energy density parameter (Ω_c) through the equation $\Omega_{m0} = \Omega_b + \Omega_c$. In four of the six models, the dark energy density parameter term is expressed as $\Omega_{\text{DE}}(z) = \Omega_{\text{DE}0}(1+z)^{1+w_{\text{DE}}}$, where $\Omega_{\text{DE}0}$ is the current value of the dark energy density parameter and w_{DE} is the dark energy equation of state parameter.

In the ΛCDM models $w_{\text{DE}} = -1$ and $\Omega_{\text{DE}} = \Omega_{\text{DE}0} = \Omega_\Lambda$ is the cosmological constant dark energy density parameter and is time-independent. The current values of the three energy density parameters are related by the energy budget equation, $\Omega_{m0} + \Omega_{k0} + \Omega_\Lambda = 1$. In the spatially-flat ΛCDM model we choose to constrain Ω_{m0} and H_0 while in the spatially non-flat ΛCDM model we constrain Ω_{m0} , Ω_{k0} , and H_0 . For analyses which involve $H(z) + \text{BAO}$ data, instead

³ For recent discussions of constraints on non-flat models see Chen et al. (2016), Rana et al. (2017), Ooba et al. (2018a,c), Yu et al. (2018), Park & Ratra (2019a,c), Wei (2018), DES Collaboration (2019), Li et al. (2020), Handley (2019), Efstathiou & Gratton (2020), Di Valentino et al. (2021a), Velasquez-Toribio & Fabris (2020), Vagnozzi et al. (2021a,b), KiDS Collaboration (2021), Arjona & Nesseris (2021), Dhawan et al. (2021), and references therein.

of Ω_{m0} we constrain Ω_bh^2 and Ω_ch^2 ; here h is the Hubble constant in units of $100 \text{ km s}^{-1} \text{ Mpc}^{-1}$.

In the XCDM parametrizations the equation of state for the dynamical dark energy X-fluid is $P_X = w_X \rho_X$ where P_X , ρ_X , and w_X are the pressure, energy density, and equation of state parameter for the dynamical dark energy X-fluid, and $\Omega_{DE0} = \Omega_{X0}$ is the current value of the X-fluid dynamical dark energy density parameter. In this case the current values of the three energy density parameters are related by $\Omega_{m0} + \Omega_{k0} + \Omega_{X0} = 1$. The X-fluid energy density decreases with time when w_X satisfies the conditions $-1 < w_X < 0$. In the spatially-flat XCDM parametrization we choose to constrain Ω_{m0} , w_X , and H_0 while in the non-flat XCDM parametrization we constrain Ω_{m0} , Ω_{k0} , w_X , and H_0 . For analyses which involve $H(z) + \text{BAO}$ data, instead of Ω_{m0} we constrain Ω_bh^2 and Ω_ch^2 . When $w_X = -1$ the XCDM parametrizations reduce to the ΛCDM models.

In the ϕCDM models the dynamical dark energy is a scalar field ϕ (Peebles & Ratra 1988; Ratra & Peebles 1988; Pavlov et al. 2013).⁴ In this model $\Omega_{DE} = \Omega_\phi(z, \alpha)$, the scalar field dynamical dark energy density parameter, is determined by the scalar field potential energy density, for which we assume an inverse power law form,

$$V(\phi) = \frac{1}{2} \kappa m_p^2 \phi^{-\alpha}. \quad (2)$$

Here m_p is the Planck mass, α is a positive parameter, and κ is a constant whose value is determined by using the shooting method to ensure that the current energy budget equation $\Omega_{m0} + \Omega_{k0} + \Omega_\phi(z=0, \alpha) = 1$ is satisfied.

In the ϕCDM models the dynamics of a spatially homogeneous scalar field ϕ is governed by two coupled non-linear ordinary differential equations. The first is the dark energy scalar field equation of motion

$$\ddot{\phi} + 3\left(\frac{\dot{a}}{a}\right)\dot{\phi} - \frac{1}{2}\alpha\kappa m_p^2\phi^{-\alpha-1} = 0, \quad (3)$$

and the second is the Friedmann equation

$$\left(\frac{\dot{a}}{a}\right)^2 = \frac{8\pi}{3m_p^2}(\rho_m + \rho_\phi) - \frac{k}{a^2}, \quad (4)$$

where a is the scale factor and an overdot denotes a time derivative. In eq. (4), $-k/a^2$ is the spatial curvature term with $\Omega_{k0} = 0, > 0, < 0$ corresponding to $k = 0, -1, +1$, respectively, and ρ_m and ρ_ϕ are the non-relativistic matter and scalar field energy densities where

$$\rho_\phi = \frac{m_p^2}{32\pi} \left(\dot{\phi}^2 + \kappa m_p^2 \phi^{-\alpha} \right). \quad (5)$$

By solving eqs. (3) and (4) numerically we can compute ρ_ϕ and then compute $\Omega_\phi(z, \alpha)$ by using the expression

$$\Omega_\phi(z, \alpha) = \frac{8\pi\rho_\phi}{3m_p^2H_0^2}. \quad (6)$$

In the spatially-flat ϕCDM model we choose to constrain

⁴ Discussions of observational constraints on the ϕCDM model can be traced through Chen et al. (2017), Zhai et al. (2017), Solà Peracaula et al. (2018, 2019), Ooba et al. (2018b, 2019), Park & Ratra (2018, 2019b, 2020), Sangwan et al. (2018), Singh et al. (2019), Ureña-López & Roy (2020), Sinha & Banerjee (2021), Cao et al. (2021c), Khadka et al. (2021a), Xu et al. (2021), de Cruz Perez et al. (2021) and references therein.

Ω_{m0} , α , and H_0 while in the non-flat ϕCDM model we constrain Ω_{m0} , Ω_{k0} , α , and H_0 . For analyses which involve $H(z) + \text{BAO}$ data, instead of Ω_{m0} we constrain Ω_bh^2 and Ω_ch^2 . When $\alpha = 0$ the ϕCDM models reduce to the ΛCDM models.

3 DATA

In this paper, we analyze four different GRB data sets as well as some combinations of these data sets. We also use a joint $H(z) + \text{BAO}$ data set. These data sets are summarized in Table 1 and described in what follows.⁵

MD-LGRB sample. This includes 31 long GRBs, with burst duration longer than 2 seconds, listed in Table 1 of Wang et al. (2021). For this data set, measured quantities for a GRB are redshift z , X-ray flux F_0 , characteristic time scale t_b , and spectral index during the plateau phase β' .⁶ This sample probes the redshift range $1.45 \leq z \leq 5.91$.

MD-SGRB sample. This includes 5 short GRBs, with burst duration shorter than 2 seconds, listed in Table 1 of Hu et al. (2021). For this data set, measured quantities for a GRB are the same as those for the MD-LGRB sample. This data set probes the redshift range $0.35 \leq z \leq 2.6$.

GW-LGRB sample. This includes 24 long GRBs listed in Table 1 of Hu et al. (2021). For this data set, measured quantities for a GRB are the same as those for the MD-LGRB sample. This sample probes the redshift range $0.55 \leq z \leq 4.81$.

A118 sample. This sample include 118 long GRBs listed in Table 7 of Khadka et al. (2021a). For this data set, measured quantities for a GRB are z , rest-frame spectral peak energy E_p , and measured bolometric fluence S_{bolo} , computed in the standard rest-frame energy band $1 - 10^4$ keV. This sample probes the redshift range $0.3399 \leq z \leq 8.2$.

The A118 data and the MD-LGRB data sets have 3 common GRBs, GRB060526, GRB081008, and GRB090516. We exclude these common GRBs from the A118 data set to form the A115 data set for joint analyses with the MD-LGRB data set. There are also 3 common GRBs between the A118 data set and the GW-LGRB data set, GRB060206, GRB091029, and GRB131105A. We exclude these common GRBs from the A118 data set to form the A115' data set for joint analyses with the GW-LGRB data set.

$H(z)$ and BAO data. In addition to the GRB data, we also use 31 $H(z)$ and 11 BAO measurements. These $H(z)$ and BAO measurements probe the redshift range $0.07 \leq z \leq 1.965$ and $0.0106 \leq z \leq 2.33$, respectively. The $H(z)$ data are in Table 2 of Ryan et al. (2018) and the BAO data are in Table 1 of Khadka & Ratra (2020c). We use cosmological

⁵ In this table and elsewhere, for compactness, we sometimes use ML, MS, and GL as abbreviations for the MD-LGRB, MD-SGRB, and GW-LGRB data sets compiled by Wang et al. (2021) and Hu et al. (2021).

⁶ ML, MS, and GL data error bars on F_0 and t_b are mostly asymmetric. We symmetrize these error bars using the method applied in Wang et al. (2021) and Hu et al. (2021), with the symmetrized error bar $\sigma = \sqrt{(\sigma_u^2 + \sigma_d^2)/2}$, where σ_u and σ_d are the asymmetric upper and lower error bars.

Table 1. Summary of data sets used.

Data set	N (Number of points)	Redshift range
ML	31	$1.45 \leq z \leq 5.91$
MS	5	$0.35 \leq z \leq 2.6$
GL	24	$0.55 \leq z \leq 4.81$
MS + GL	29	$0.35 \leq z \leq 4.81$
A118	118	$0.3399 \leq z \leq 8.2$
A115 ^a	115	$0.3399 \leq z \leq 8.2$
A115' ^b	115	$0.3399 \leq z \leq 8.2$
$H(z)$	31	$0.070 \leq z \leq 1.965$
BAO	11	$0.38 \leq z \leq 2.334$

^a Excluding from A118 those GRBs in common with MD-LGRB (GRB060526, GRB081008, and GRB090516).

^b Excluding from A118 those GRBs in common with GW-LGRB (GRB060206, GRB091029, and GRB131105A).

Table 2. Flat priors of the constrained parameters.

Parameter	Prior
Cosmological Parameters	
H_0 ^a	[None, None]
$\Omega_b h^2$ ^b	[0, 1]
$\Omega_c h^2$ ^c	[0, 1]
Ω_{k0}	[-2, 2]
α	[0, 10]
w_X	[-5, 0.33]
GRB Nuisance Parameters ^d	
k	[-10, 10]
b ^e	[0, 10]
σ_{int}	[0, 5]
β	[0, 5]
γ	[0, 300]

^a $\text{km s}^{-1} \text{Mpc}^{-1}$. In the GRB alone cases, H_0 is set to be $70 \text{ km s}^{-1} \text{Mpc}^{-1}$, while in the $H(z) + \text{BAO}$ case, the prior range is irrelevant (unbounded).

^b In the GRB alone cases, $\Omega_b h^2$ is set to be 0.0245, i.e. $\Omega_b = 0.05$.

^c In the GRB alone cases, $\Omega_c \in [-0.05, 0.95]$ to ensure $\Omega_{m0} \in [0, 1]$.

^d Note that k , b , and σ_{int} of MD-LGRBs are different from those of MD-SGRBs/GW-LGRBs, but with the same prior ranges.

^e $b < 0$ values are possible for MD-SGRBs (due to fewer data points) but, as discussed below, requiring $b \geq 0$ does not have significant consequences.

constraints from the better-established $H(z) + \text{BAO}$ data to compare with those obtained from the GRB data sets.

4 DATA ANALYSIS METHODOLOGY

For GRBs which obey the Dainotti correlation the luminosity of the plateau phase is (Dainotti et al. 2008, 2010, 2011)

$$L_0 = \frac{4\pi D_L^2 F_0}{(1+z)^{1-\beta'}}, \quad (7)$$

where F_0 is the GRB X-ray flux, β' is the spectral index in the plateau phase, and D_L is the luminosity distance.

D_L , as a function of redshift z and cosmological parameters \mathbf{p} , is given by

$$H_0 \sqrt{|\Omega_{k0}|} D_L(z, \mathbf{p}) = \begin{cases} \sinh[g(z, \mathbf{p})] & \text{if } \Omega_{k0} > 0, \\ g(z, \mathbf{p}) & \text{if } \Omega_{k0} = 0, \\ \sin[g(z, \mathbf{p})] & \text{if } \Omega_{k0} < 0, \end{cases} \quad (8)$$

where

$$g(z, \mathbf{p}) = H_0 \sqrt{|\Omega_{k0}|} \int_0^z \frac{dz'}{H(z', \mathbf{p})}, \quad (9)$$

c is the speed of light, and $H(z, \mathbf{p})$ is the Hubble parameter that is described in Sec. 2 for each cosmological model.

For these GRBs the luminosity of the plateau phase L_0 and the characteristic time scale t_b are correlated through the Dainotti or luminosity-time relation

$$y \equiv \log \left(\frac{L_0}{10^{47} \text{ erg/s}} \right) = k \log \frac{t_b}{10^3 (1+z) \text{ s}} + b \equiv kx + b, \quad (10)$$

where $\log = \log_{10}$ and the slope k and the intercept b are free parameters to be determined from the data.

We predict L_0 as a function of cosmological parameters \mathbf{p} at the redshift of each GRB by using eqs. (7), (8), and (10). We then compare predicted and measured values of L_0 by using the natural log of the likelihood function (D’Agostini 2005)

$$\ln \mathcal{L}_{\text{GRB}} = -\frac{1}{2} \left[\chi_{\text{GRB}}^2 + \sum_{i=1}^N \ln (2\pi(\sigma_{\text{int}}^2 + \sigma_{y_i}^2 + k^2 \sigma_{x_i}^2)) \right], \quad (11)$$

where

$$\chi_{\text{GRB}}^2 = \sum_{i=1}^N \left[\frac{(y_i - kx_i - b)^2}{(\sigma_{\text{int}}^2 + \sigma_{y_i}^2 + k^2 \sigma_{x_i}^2)} \right]. \quad (12)$$

Here N is the number of data points (e.g., for MD-LGRB $N = 31$), and σ_{int} is the intrinsic scatter parameter (which also contains the unknown systematic uncertainty).

For GRBs which obey the Amati correlation the rest frame isotropic radiated energy E_{iso} is

$$E_{\text{iso}} = \frac{4\pi D_L^2}{1+z} S_{\text{bolo}}, \quad (13)$$

where S_{bolo} is the bolometric fluence.

For these GRBs the rest frame peak photon energy E_p and E_{iso} are correlated through the Amati (or $E_p - E_{\text{iso}}$) relation (Amati et al. 2008, 2009)

$$\log E_{\text{iso}} = \gamma + \beta \log E_p, \quad (14)$$

where the intercept γ and the slope β are free parameters to be determined from the data. Note that the peak energy $E_p = (1+z)E_{p,\text{obs}}$ where $E_{p,\text{obs}}$ is the observed peak energy.

We predict E_{iso} as a function of cosmological parameters \mathbf{p} at the redshift of each GRB by using eqs. (8), (13), and (14). We then compare predicted and measured values of E_{iso} by using the natural log of the likelihood function (D’Agostini 2005)

$$\ln \mathcal{L}_{\text{A118}} = -\frac{1}{2} \left[\chi_{\text{A118}}^2 + \sum_{i=1}^N \ln (2\pi(\sigma_{\text{int}}^2 + \sigma_{y'_i}^2 + \beta^2 \sigma_{x'_i}^2)) \right], \quad (15)$$

(15)

where

$$\chi^2_{\text{A}118} = \sum_{i=1}^N \left[\frac{(y'_i - \beta x'_i - \gamma)^2}{(\sigma_{\text{int}}^2 + \sigma_{y'_i}^2 + \beta^2 \sigma_{x'_i}^2)} \right]. \quad (16)$$

Here $x' = \log(E_{\text{p}}/\text{keV})$, $\sigma_{x'} = \sigma_{E_{\text{p}}} / (E_{\text{p}} \ln 10)$, $y' = \log(E_{\text{iso}}/\text{erg})$, and σ_{int} is the intrinsic scatter parameter, which also contains the unknown systematic uncertainty.

The $H(z) + \text{BAO}$ data analyses follow the method described in Sec. 4 of Khadka & Ratra (2021a).

We maximize the likelihood function using the Markov chain Monte Carlo (MCMC) method as implemented in the MONTEPYTHON code (Brinckmann & Lesgourgues 2019) and determine the best-fitting and posterior mean values and the corresponding uncertainties for all free parameters. We assure convergence of the MCMC chains for each free parameter from the Gelman-Rubin criterion ($R-1 < 0.05$). Flat priors used for the free parameters are given in Table 2.

The Akaike Information Criterion (AIC) and the Bayesian Information Criterion (BIC) are used to compare the goodness of fit of models with different numbers of parameters. These are

$$AIC = -2 \ln \mathcal{L}_{\text{max}} + 2n, \quad (17)$$

and

$$BIC = -2 \ln \mathcal{L}_{\text{max}} + n \ln N. \quad (18)$$

In these equations, \mathcal{L}_{max} is the maximum value of the relevant likelihood function and n is the number of free parameters of the model under consideration.

5 RESULTS

5.1 Constraints from ML, MS, and GL data

In Table 3 we list Dainotti correlation parameters computed using the ML, GL, and MS data sets. These are computed in the flat ΛCDM model with $\Omega_{\text{m}0} = 0.3$ and $H_0 = 70 \text{ km s}^{-1} \text{ Mpc}^{-1}$, the same model and parameter values used in Wang et al. (2021) and Hu et al. (2021). The first line of parameter values in each of the three subpanels of Table 3 are taken from these papers.⁷ To compare to these results, we used EMCEE (Foreman-Mackey et al. 2013) to compute the values listed in the second and third lines of each subpanel. Comparing the first and second lines in each subpanel, we find that they are consistent, except: i) for the GL case our b uncertainties are larger than those of Hu et al. (2021); and, ii) for the MS case we have larger b and k error bars and a larger central value of σ_{int} than those of Hu et al. (2021), but they agree within 1σ . In the third line of each subpanel we list results obtained assuming wider prior ranges of the parameters. We find that the ML results do not change, the GL results are shifted closer to those of Hu et al. (2021), except for the values of σ_{int} , and the MS results are shifted away from those of Hu et al. (2021) with larger error bars, especially for σ_{int} .

We now record and discuss results when these data sets

⁷ Wang et al. (2021) do not list a value for σ_{int} in the ML case.

Table 3. One-dimensional marginalized posterior means and 68.27% limits of the Dainotti correlation parameters for the ML, GL, and MS data sets using the flat ΛCDM model with $\Omega_{\text{m}0} = 0.3$ and $H_0 = 70 \text{ km s}^{-1} \text{ Mpc}^{-1}$, and comparison with the results given in Wang et al. (2021) and Hu et al. (2021).

Data set	Source	k	b	σ_{int}
ML	a	$-1.02^{+0.09}_{-0.08}$	$1.72^{+0.07}_{-0.07}$	—
	b	-1.026 ± 0.085	1.726 ± 0.074	$0.303^{+0.032}_{-0.050}$
	c	-1.026 ± 0.086	1.726 ± 0.074	$0.303^{+0.032}_{-0.050}$
GL	d	$-1.77^{+0.20}_{-0.20}$	$0.66^{+0.01}_{-0.01}$	$0.42^{+0.08}_{-0.06}$
	b	$-1.753^{+0.187}_{-0.208}$	$0.642^{+0.100}_{-0.071}$	$0.428^{+0.053}_{-0.086}$
	c	-1.769 ± 0.205	0.656 ± 0.094	$0.431^{+0.054}_{-0.088}$
MS	d	$-1.38^{+0.17}_{-0.19}$	$0.33^{+0.17}_{-0.16}$	$0.35^{+0.20}_{-0.12}$
	b	$-1.381^{+0.209}_{-0.213}$	$0.327^{+0.195}_{-0.189}$	$0.420^{+0.086}_{-0.242}$
	c	$-1.397^{+0.247}_{-0.241}$	$0.354^{+0.195}_{-0.242}$	$0.525^{+0.044}_{-0.358}$

^a Results from Wang et al. (2021) with the prior ranges of the parameters being $k \in (-1.3, -0.75)$, $b \in (1.4, 2.0)$, and $\sigma_{\text{int}} \in (0.1, 0.6)$ for ML.

^b Our results with the same prior ranges of the parameters as Wang et al. (2021) or Hu et al. (2021).

^c Our results with wider prior ranges of the parameters $k \in [-10, 10]$, $b \in [0, 10]$ ($b \in [-0.5, 10]$), and $\sigma_{\text{int}} \in [0, 3]$ for ML and GL (MS).

^d Results from Hu et al. (2021) with the prior ranges of the parameters being $k \in (-2.2, -1)$, $b \in (0.1, 0.8)$, and $\sigma_{\text{int}} \in (0.01, 0.8)$ for GL and being $k \in (-2.1, -0.55)$, $b \in (-0.5, 1.0)$, and $\sigma_{\text{int}} \in (0.01, 1)$ for MS.

are used to jointly constrain the Dainotti parameters and the cosmological parameters of the six spatially-flat and non-flat dark energy cosmological models. Figure 1 shows the flat ΛCDM Dainotti correlations for the ML, MS, GL, and MS + GL data sets. The unmarginalized best-fitting results and the one-dimensional (1D) posterior mean values and uncertainties are reported in Tables 4 and 5, respectively. The corresponding posterior 1D probability distributions and two-dimensional (2D) confidence regions of these parameters are shown in Figs. 2–4, in blue (ML), gray (MS), green (GL), pink (ML + MS), violet (ML + GL), orange (MS + GL), and red ($H(z) + \text{BAO}$, as a baseline). Note that $H_0 = 70 \text{ km s}^{-1} \text{ Mpc}^{-1}$ and $\Omega_b = 0.05$ are applied in the GRB cases.

ML, MS, and GL GRB data have almost cosmological-model independent Dainotti parameters. This means that it is not unreasonable to treat the ML, MS, and GL GRBs as standardizable candles, as was assumed in Wang et al. (2021) and Hu et al. (2021).

In the ML case (with subscript “ML” in the first line of Tables 4, 5, 7, and 8), the slope k ranges from a high of -0.996 ± 0.097 (non-flat XCDM) to a low of -1.017 ± 0.090 (flat ΛCDM), the intercept b ranges from a high of $1.611^{+0.113}_{-0.277}$ (flat XCDM) to a low of $1.448^{+0.120}_{-0.165}$ (non-flat ϕCDM), and the intrinsic scatter σ_{int} ranges from a high of $0.306^{+0.036}_{-0.054}$ (flat XCDM) to a low of $0.303^{+0.035}_{-0.053}$ (non-flat ϕCDM), with central values of each pair being 0.16σ , 0.54σ , and 0.05σ away from each other, respectively.

In the MS case (with subscript “MS” in the first line of Tables 4 and 5) with prior range of $b \in [0, 10]$, the slope k ranges from a high of $-1.425^{+0.311}_{-0.221}$ (flat ϕCDM) to a low of $-1.450^{+0.362}_{-0.258}$ (flat ΛCDM), the intercept b ranges from a high of $0.497^{+0.086}_{-0.458}$ (flat XCDM) to a low of $0.352^{+0.048}_{-0.331}$ (non-

Table 4: Unmarginalized best-fitting parameter values for all models from various combinations of data.

Model	Data set	$\Omega_b h^2$	$\Omega_{\text{m}0}$	Ω_{k0}	w_X	α	H_0^{a}	$\sigma_{\text{int}, \text{MS}}$	b_{MS}	k_{MS}	$\sigma_{\text{int}, \text{GL}}$	b_{GL}	k_{GL}	$\sigma_{\text{int}, \text{MS+GL}}$	$b_{\text{MS+GL}}$	$k_{\text{MS+GL}}$	AIC	BIC	ΔAIC	ΔBIC			
Flat Λ CDM	$H(z) + \text{BAO}$	0.0239	0.1187	0.298	—	—	69.13	—	—	—	—	—	—	—	—	—	23.66	29.66	34.87	0.00			
	ML	0.0245	0.4645	0.998	—	—	70	0.275	1.383	-1.010	—	—	—	—	—	—	8.68	16.68	22.41	0.00			
	MS	0.0245	0.4651	0.999	—	—	70	—	—	0.159	0.105	-1.310	—	—	—	—	-3.49	4.51	2.95	0.00			
	GL	0.0245	0.4641	0.997	—	—	70	—	—	—	—	0.370	0.359	-1.675	—	—	-22.94	30.94	35.65	0.00			
	MS + GL	0.0245	0.4652	0.999	—	—	70	—	—	—	—	0.329	0.238	-1.377	—	—	17.00	27.00	32.89	-10.32			
	ML + GL	0.0245	0.4642	0.997	—	—	70	0.274	1.378	-1.008	—	—	0.361	0.313	-1.545	—	—	16.92	26.02	31.91	-10.71		
Non-flat Λ CDM	MS + GL	0.0245	0.4649	0.999	-1.738	—	70	—	—	—	—	—	—	—	—	—	17.00	27.00	32.89	-10.32			
	ML + GL	0.0245	0.4330	0.934	-1.298	—	70	0.269	1.248	-0.953	—	—	0.336	0.330	-1.529	—	—	26.79	42.79	58.84	-2.76		
	ML + MS	0.0245	0.4625	0.994	-1.130	—	70	0.259	1.278	-0.966	0.136	0.159	-1.249	—	—	—	—	2.91	18.91	31.58	-0.43		
	$H(z) + \text{BAO}$	0.0247	0.1140	0.294	0.029	—	68.68	—	—	—	—	—	—	—	—	—	23.60	31.60	38.55	1.94			
	ML	0.0245	0.4410	0.950	-0.973	—	70	0.268	1.316	-0.967	—	0.007	0.023	-0.919	—	—	—	—	7.48	17.48	24.65	0.80	
	MS	0.0245	0.2727	0.067	-1.730	—	70	—	—	—	—	0.329	0.238	-1.377	—	—	-15.81	-5.81	-7.76	-10.71			
Flat XCDM	MS + GL	0.0245	0.4640	0.997	-1.703	—	70	—	—	—	—	0.304	0.220	-1.303	—	—	27.00	32.89	38.30	0.00			
	ML + GL	0.0245	0.4652	0.999	-1.738	—	70	—	—	—	—	—	—	—	—	—	16.92	26.02	31.91	-10.71			
	ML + MS	0.0245	0.463	0.995	—	—	70	0.274	1.388	-1.013	0.148	0.080	-1.322	—	—	—	5.34	19.34	30.42	0.00			
	$H(z) + \text{BAO}$	0.0247	0.1140	0.294	0.029	—	68.68	—	—	—	—	—	—	—	—	—	23.60	31.60	38.55	1.94			
	ML	0.0245	0.4410	0.950	-0.973	—	70	0.268	1.316	-0.967	—	0.007	0.023	-0.919	—	—	—	—	7.48	17.48	24.65	0.80	
	MS	0.0245	0.067	-1.607	-1.730	—	70	—	—	—	—	0.329	0.238	-1.377	—	—	-15.81	-5.81	-7.76	-10.71			
Non-flat XCDM	MS + GL	0.0245	0.4649	0.999	-1.738	—	70	—	—	—	—	—	—	—	—	—	17.00	27.00	32.89	-10.71			
	ML + GL	0.0245	0.4330	0.934	-1.298	—	70	0.269	1.248	-0.953	—	0.159	-1.249	—	—	—	16.92	26.02	31.91	-10.71			
	ML + MS	0.0245	0.4625	0.994	-1.130	—	70	0.259	1.278	-0.966	0.136	0.159	-1.249	—	—	—	2.91	18.91	31.58	-0.43			
	$H(z) + \text{BAO}$	0.0247	0.0891	0.281	—	-0.701	—	65.18	—	—	—	—	—	—	—	—	19.65	27.65	34.60	-2.01			
	ML	0.0245	0.0327	0.117	—	0.133	—	70	0.275	1.288	-0.957	—	—	—	—	—	8.14	18.14	25.31	1.46			
	MS	0.0245	0.0339	0.042	—	0.141	—	70	—	—	0.160	0.054	-1.285	—	—	—	-4.23	5.77	3.81	0.86			
Flat ϕ CDM	MS + GL	0.0245	0.0035	0.057	—	0.139	—	70	—	—	—	—	0.364	0.259	-1.651	—	—	21.97	31.97	37.86	1.93		
	ML + GL	0.0245	0.0058	0.062	—	0.141	—	70	—	—	—	—	—	0.346	0.248	-1.518	—	—	23.92	33.92	39.81	0.33	
	ML + MS	0.0245	0.0735	0.200	—	0.143	—	70	0.273	1.300	-1.015	—	0.359	0.273	-1.636	—	—	30.20	46.20	62.26	0.54		
	$H(z) + \text{BAO}$	0.0245	-0.0207	0.008	—	0.137	—	70	0.278	1.269	-0.984	0.175	0.031	-1.282	—	—	—	3.99	19.99	32.65	0.65		
	ML	0.0245	0.0290	0.0980	0.295	-0.152	-0.655	—	65.59	—	—	—	—	—	—	—	—	18.31	28.31	37.00	-1.35		
	MS	0.0245	0.1525	0.361	-1.893	—	70	0.269	0.949	-0.976	—	0.057	0.098	-0.995	—	—	—	—	7.39	19.39	27.99	2.71	
Non-flat ϕ CDM	GL	0.0245	0.3576	0.784	-1.915	—	70	—	—	—	—	0.327	0.237	-1.237	—	—	-13.61	-1.61	-3.95	-6.90			
	MS + GL	0.0245	0.3978	0.127	-1.714	-4.518	—	70	—	—	—	—	—	—	—	—	16.61	28.61	35.68	-2.33			
	ML + GL	0.0245	0.4212	0.910	-1.218	-2.308	—	70	—	—	—	—	—	—	—	—	26.04	44.04	56.65	-3.58			
	ML + MS	0.0245	0.3594	0.783	-0.789	-4.432	—	70	0.269	1.449	-0.927	—	0.338	0.576	-1.429	—	—	26.04	44.04	62.11	-1.62		
	$H(z) + \text{BAO}$	0.0245	0.0333	0.0788	0.264	—	—	—	—	—	—	—	—	—	—	—	—	17.96	32.21	38.38	1.79		
	ML	0.0245	0.4651	0.999	—	5.325	70	0.275	1.383	-1.011	—	0.160	0.099	-1.306	—	—	—	—	19.49	27.49	34.44	-2.17	
Non-flat ϕ CDM	MS	0.0245	0.4649	0.999	—	8.046	70	—	—	—	0.160	—	0.372	0.360	-1.674	—	—	—	—	8.68	18.68	25.85	2.00
	GL	0.0245	0.4641	0.997	—	4.299	70	—	—	—	—	—	—	0.372	0.360	-1.674	—	—	-3.49	6.51	45.6	2.00	
	MS + GL	0.0245	0.4653	1.000	—	6.323	70	—	—	—	—	—	—	0.359	0.314	-1.545	—	—	22.94	32.94	38.83	2.00	
	ML + GL	0.0245	0.4638	0.999	—	7.886	70	0.274	1.375	-1.013	—	0.113	-1.317	—	0.333	-1.647	—	—	31.72	41.48	51.59	3.18	
	ML + MS	0.0245	0.4611	0.991	—	6.029	70	0.268	1.371	-0.997	0.148	—	0.371	—	—	—	—	5.32	21.32	33.99	1.98		
	$H(z) + \text{BAO}$	0.0245	0.0334	0.0816	0.266	-0.147	—	1.915	65.70	—	—	—	—	—	—	—	—	18.15	28.15	36.84	-1.51		
Non-flat ϕ CDM	ML	0.0245	0.4558	0.980	-0.980	—	0.423	70	0.266	1.296	-0.973	—	0.132	0.093	-1.261	—	—	—	—	7.48	19.48	28.09	5.68
	MS	0.0245	0.4482	0.965	-0.964	—	8.262	70	—	—	—	—	—	—	—	—	-5.25	6.75	4.40	2.24			
	GL	0.0245	0.4644	0.998	-0.993	—	0.173	70	—	—	—	0.340	0.337	-1.547	—	—	20.15	32.15	39.22	1.21			
	MS + GL	0.0245	0.4601	0.989	-0.982	—	0.011	70	—	—	—	—	—	0.315	0.310	-1.484	—	—	33.46	40.53	-0.13	2.23	
	ML + GL	0.0245	0.4465	0.961	-0.950	—	0.232	70	0.255	1.290	-0.969	—	0.348	0.356	-1.600	—	—	28.04	46.04	64.11	0.38		
	ML + MS	0.0245	0.4628	0.995	-0.936	—	8.517	70	0.281	1.202	-0.994	0.152	0.027	-1.291	—	—	—	—	2.71	20.71	34.96	1.36	

^a $\text{km s}^{-1} \text{Mpc}^{-1}$. In the GRB only cases, H_0 is set to be $70 \text{ km s}^{-1} \text{Mpc}^{-1}$.

Table 5: One-dimensional marginalized posterior mean values and uncertainties ($\pm 1\sigma$ error bars or 2σ limits) of the parameters for all models from various combinations of data.

Model	Data set	$Q_0 k^2$	$Q_0 h^2$	Q_{00}	Q_{00}	Ω_m	Ω_m	H_0^a	$\sigma_{\text{int}, \text{M}}$	b_{M}	b_{M}	$\sigma_{\text{int}, \text{GL}}$	b_{GL}	$b_{\text{int}, \text{M+GL}}$	$k_{\text{M+GL}}$
Flat Λ CDM	$H(z)$ + BAO	0.0241 \pm 0.0029	0.1183 \pm 0.0082	0.296 \pm 0.017	> 0.188	-	-	69.30 \pm 1.84	-	-	-	-	-	-	-
	ML	-	-	0.520 \pm 0.233	0.520 \pm 0.379	-	-	-	0.365 \pm 0.053	1.557 \pm 0.08	-1.07 \pm 0.090	-	-	-	-
	MS	-	-	-	-	-	-	-	-	-	0.686 \pm 0.59	0.437 \pm 0.73	-1.450 \pm 0.38	-	-
	GL	-	-	-	-	-	-	-	-	-	-	0.429 \pm 0.69	0.405 \pm 0.173	-1.720 \pm 0.219	-
	MS + GL	-	-	-	-	-	-	-	-	-	-	0.402 \pm 0.060	0.421 \pm 0.101	-1.577 \pm 0.155	-
	ML + GL	-	-	-	-	-	-	-	-	-	-	0.322 \pm 0.034	0.405 \pm 0.113	0.421 \pm 0.052	0.421 \pm 0.141
	ML + MS	-	-	-	-	-	-	-	-	-	-	0.302 \pm 0.032	0.405 \pm 0.149	-1.708 \pm 0.210	-
Non-flat Λ CDM	$H(z)$ + BAO	0.0253 \pm 0.0041	0.1135 \pm 0.0196	0.283 \pm 0.025	0.309 \pm 0.115	-	-	68.75 \pm 2.37	-	-	-	-	-	-	-
	ML	-	-	> 0.241	-0.131 \pm 0.350	-	-	-	0.364 \pm 0.053	1.478 \pm 0.123	-1.000 \pm 0.096	-	-	-	-
	MS	-	-	-	0.564 \pm 0.426	-0.066 \pm 1.092	-	-	-	-	0.670 \pm 0.024	0.413 \pm 0.393	-1.430 \pm 0.360	-	
	GL	-	-	-	0.564 \pm 0.449	-0.066 \pm 1.199	-	-	-	-	0.402 \pm 0.057	0.407 \pm 0.136	-1.536 \pm 0.252	-	
	MS + GL	-	-	-	> 0.290	-0.176 \pm 0.888	-	-	-	-	-	0.402 \pm 0.060	0.407 \pm 0.160	0.357 \pm 0.06	0.357 \pm 0.110
	ML + GL	-	-	-	> 0.391	-1.165 \pm 0.515	-	-	-	-	-	0.300 \pm 0.051	1.386 \pm 0.138	-1.588 \pm 0.25	-1.382 \pm 0.164
Flat XCDM	$H(z)$ + BAO	0.0296 \pm 0.0046	0.0939 \pm 0.0194	0.284 \pm 0.023	-	-	-	65.80 \pm 2.41	-	-	-	-	-	-	-
	ML	-	-	-	-	-	-	-	0.366 \pm 0.054	1.611 \pm 0.113	-1.014 \pm 0.092	-	-	-	-
	MS	-	-	-	0.320 \pm 0.340	-2.494 \pm 2.180	-	-	-	0.704 \pm 0.035	0.497 \pm 0.086	-1.441 \pm 0.366	-	-	
	GL	-	-	-	> 0.141	-2.494 \pm 2.050	-	-	-	-	0.428 \pm 0.058	0.556 \pm 0.127	-1.706 \pm 0.215	-	
	MS + GL	-	-	-	> 0.192	-	-	-	-	-	-	0.300 \pm 0.051	1.566 \pm 0.099	0.409 \pm 0.052	0.409 \pm 0.108
	ML + GL	-	-	-	> 0.164	-	-	-	-	-	-	0.302 \pm 0.052	1.457 \pm 0.128	-1.700 \pm 0.206	-1.570 \pm 0.155
Non-flat XCDM	$H(z)$ + BAO	0.0290 \pm 0.0052	0.0939 \pm 0.0171	0.284 \pm 0.021	-	-	-	65.80 \pm 2.41	-	-	-	-	-	-	-
	ML	-	-	-	> 0.123	-2.466 \pm 2.067	-	-	-	0.366 \pm 0.054	1.611 \pm 0.113	-1.014 \pm 0.092	-	-	
	MS	-	-	-	0.320 \pm 0.276	-2.494 \pm 2.050	-	-	-	-	0.704 \pm 0.034	0.497 \pm 0.058	-1.441 \pm 0.366	-	
	GL	-	-	-	< 0.046	-	-	-	-	-	-	0.428 \pm 0.058	0.556 \pm 0.256	-1.706 \pm 0.215	-
	MS + GL	-	-	-	< 0.028	-	-	-	-	-	-	0.300 \pm 0.053	1.566 \pm 0.099	0.409 \pm 0.052	0.409 \pm 0.108
	ML + GL	-	-	-	< 0.022	-	-	-	-	-	-	0.303 \pm 0.051	1.566 \pm 0.099	-1.501 \pm 0.239	-1.501 \pm 0.266
Non-flat ϕ CDM	$H(z)$ + BAO	0.0290 \pm 0.0052	0.0990 \pm 0.0214	0.283 \pm 0.028	-0.116 \pm 0.134	-0.700 \pm 0.138	-	65.96 \pm 2.32	-	-	-	-	-	-	-
	ML	-	-	-	-	-	-	-	0.365 \pm 0.054	1.462 \pm 0.194	-0.996 \pm 0.097	-	-	-	-
	MS	-	-	-	-	-	-	-	-	-	0.733 \pm 0.031	0.464 \pm 0.444	-1.433 \pm 0.394	-	
	GL	-	-	-	-	-	-	-	-	-	-	0.403 \pm 0.058	0.480 \pm 0.270	-1.532 \pm 0.259	-
	MS + GL	-	-	-	-	-	-	-	-	-	-	0.308 \pm 0.053	0.480 \pm 0.223	-1.532 \pm 0.260	-1.538 \pm 0.175
	ML + GL	-	-	-	-	-	-	-	-	-	-	0.301 \pm 0.051	1.422 \pm 0.201	-1.561 \pm 0.220	-1.561 \pm 0.19
Non-flat ϕ CDM	$H(z)$ + BAO	0.0321 \pm 0.0056	0.0823 \pm 0.0186	0.268 \pm 0.024	-	-	-	65.96 \pm 2.32	-	-	-	-	-	-	-
	ML	-	-	-	-	-	-	-	0.364 \pm 0.054	1.462 \pm 0.194	-0.996 \pm 0.097	-	-	-	-
	MS	-	-	-	-	-	-	-	-	-	0.733 \pm 0.031	0.464 \pm 0.444	-1.433 \pm 0.394	-	
	GL	-	-	-	-	-	-	-	-	-	-	0.403 \pm 0.058	0.480 \pm 0.270	-1.532 \pm 0.259	-
	MS + GL	-	-	-	-	-	-	-	-	-	-	0.308 \pm 0.053	0.480 \pm 0.223	-1.532 \pm 0.260	-1.538 \pm 0.175
	ML + GL	-	-	-	-	-	-	-	-	-	-	0.301 \pm 0.051	1.422 \pm 0.201	-1.561 \pm 0.220	-1.561 \pm 0.19
Non-flat ϕ CDM	$H(z)$ + BAO	0.0319 \pm 0.0062	0.0823 \pm 0.0183	0.268 \pm 0.024	-	-	-	65.96 \pm 2.32	-	-	-	-	-	-	-
	ML	-	-	-	-	-	-	-	0.364 \pm 0.054	1.462 \pm 0.194	-0.996 \pm 0.097	-	-	-	-
	MS	-	-	-	-	-	-	-	-	-	0.733 \pm 0.031	0.464 \pm 0.444	-1.433 \pm 0.394	-	
	GL	-	-	-	-	-	-	-	-	-	-	0.403 \pm 0.058	0.480 \pm 0.270	-1.532 \pm 0.259	-
	MS + GL	-	-	-	-	-	-	-	-	-	-	0.308 \pm 0.053	0.480 \pm 0.223	-1.532 \pm 0.260	-1.538 \pm 0.175
	ML + MS	-	-	-	-	-	-	-	-	-	-	0.301 \pm 0.051	1.422 \pm 0.201	-1.561 \pm 0.220	-1.561 \pm 0.19
Non-flat ϕ CDM	$H(z)$ + BAO	0.0319 \pm 0.0062	0.0848 \pm 0.0181	0.271 \pm 0.025	-0.074 \pm 0.104	-0.271 \pm 0.028	-	65.96 \pm 2.31	-	-	-	-	-	-	-
	ML	-	-	-	-	-	-	-	0.365 \pm 0.054	1.462 \pm 0.194	-0.996 \pm 0.097	-	-	-	-
	MS	-	-	-	-	-	-	-	-	-	0.733 \pm 0.031	0.464 \pm 0.444	-1.433 \pm 0.394	-	
	GL	-	-	-	-	-	-	-	-	-	-	0.403 \pm 0.058	0.480 \pm 0.270	-1.532 \pm 0.259	-
	MS + GL	-	-	-	-	-	-	-	-	-	-	0.308 \pm 0.053	0.480 \pm 0.223	-1.532 \pm 0.260	-1.538 \pm 0.175
	ML + GL	-	-	-	-	-	-	-	-	-	-	0.301 \pm 0.051	1.422 \pm 0.201	-1.561 \pm 0.220	-1.561 \pm 0.19
Non-flat ϕ CDM	$H(z)$ + BAO	0.0319 \pm 0.0062	0.0848 \pm 0.0220	0.271 \pm 0.025	-0.074 \pm 0.104	-0.271 \pm 0.028	-	65.96 \pm 2.31	-	-	-	-	-	-	-
	ML	-	-	-	-	-	-	-	0.365 \pm 0.054	1.462 \pm 0.194	-0.996 \pm 0.097	-	-	-	-
	MS	-	-	-	-	-	-	-	-	-	0.733 \pm 0.031	0.464 \pm 0.444	-1.433 \pm 0.394	-	
	GL	-	-	-	-	-	-	-	-	-	-	0.403 \pm 0.058	0.480 \pm 0.270	-1.532 \pm 0.259	-
	MS + GL	-	-	-	-	-	-	-	-	-	-	0.308 \pm 0.053	0.480 \pm 0.223	-1.532 \pm 0.260	-1.538 \pm 0.175
	ML + MS	-	-	-	-	-	-	-	-	-	-	0.301 \pm 0.051	1.422 \pm 0.201	-1.561 \pm 0.220	-1.561 \pm 0.19
Non-flat ϕ CDM	$H(z)$ + BAO	0.0319 \pm 0.0062	0.0848 \pm 0.0181	0.271 \pm 0.025	-0.074 \pm 0.104	-0.271 \pm 0.028	-	65.96 \pm 2.31	-	-	-	-	-	-	-
	ML	-	-	-	-	-	-	-	0.365 \pm 0.054	1.462 \pm 0.194	-0.996 \pm 0.097	-	-	-	-
	MS	-	-	-	-	-	-	-	-	-	0.733 \pm 0.031	0.464 \pm 0.444	-1.433 \pm 0.394	-	
	GL	-	-	-	-	-	-	-	-	-	-	0.403 \pm 0.058	0.480 \pm 0.270	-1.532 \pm 0.259	-
	MS + GL	-	-	-	-	-	-	-	-	-	-	0.308 \pm 0.053	0.480 \pm 0.223	-1.532 \pm 0.260	-1.538 \pm 0.175
	ML + MS	-	-	-	-	-	-	-	-	-	-	0.301 \pm 0.051	1.422 \pm 0.201	-1.561 \pm 0.220	-1.561 \pm 0.19
Non-flat ϕ CDM	$H(z)$ + BAO	0.0319 \pm 0.0062	0.0848 \pm 0.0181	0.271 \pm 0.025	-0.074 \pm 0.104	-0.271 \pm 0.028	-	65.96 \pm 2.31	-	-	-	-	-	-	-
	ML	-	-	-	-	-	-	-	0.365 \pm 0.054	1.462 \pm 0.194	-0.996 \pm 0.097	-	-	-	-
	MS	-	-	-	-	-</td									

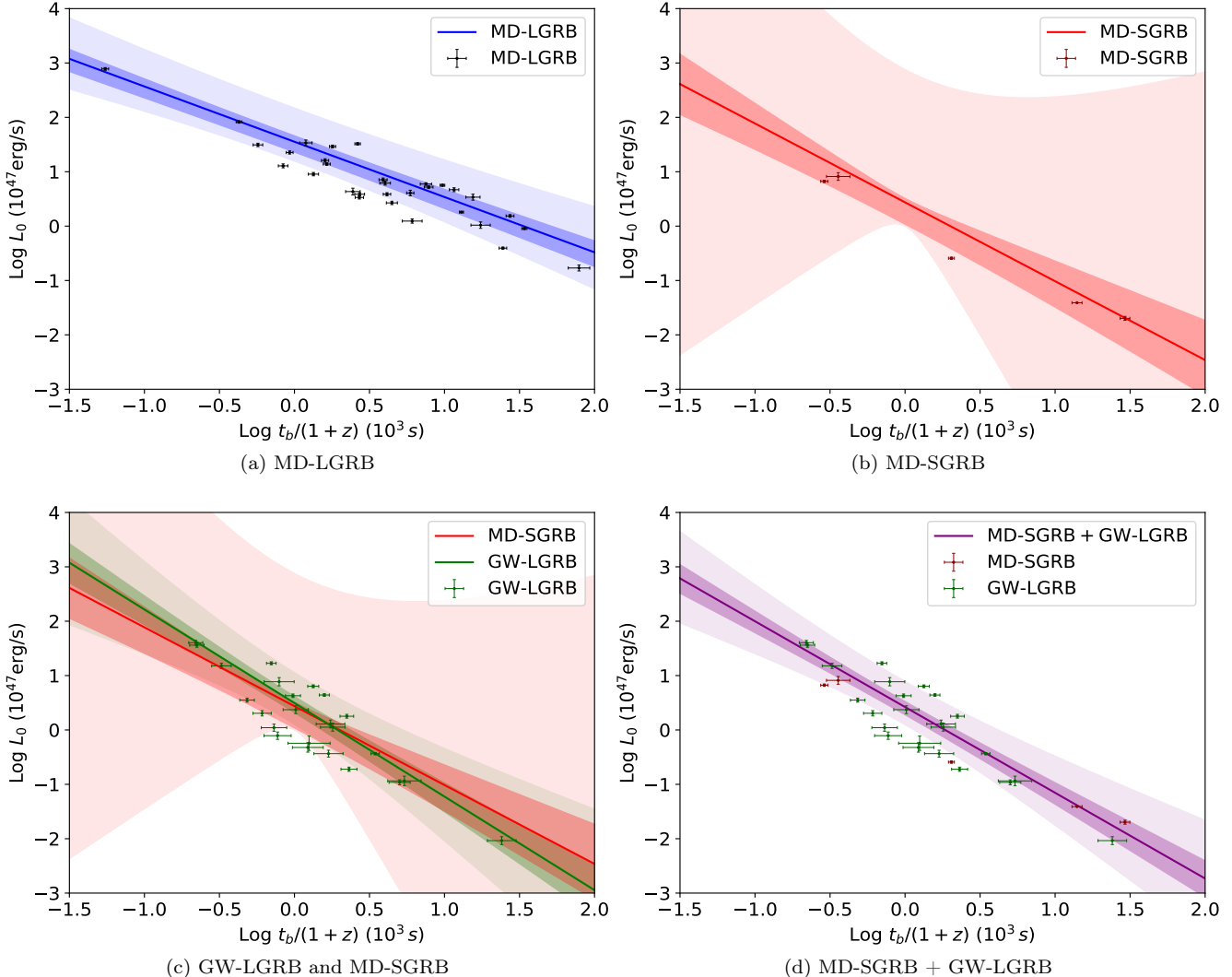


Figure 1. $L_0 - t_b$ correlations for MD-LGRB, MD-SGRB, GW-LGRB, and MD-SGRB + GW-LGRB data using the flat Λ CDM model. The MD-LGRB, MD-SGRB, and GW-LGRB data with error bars are shown in black, dark red, and dark green, respectively. The solid lines are the $L_0 - t_b$ correlations with posterior mean values for the slopes and intercepts listed in Table 5, for MD-LGRB (blue), MD-SGRB (red), GW-LGRB (green), and MD-SGRB + GW-LGRB (purple) data. The 1σ and 3σ confidence regions are the dark and light colored shaded regions with the uncertainties propagated from those of k and b (without considering σ_{int}).

flat ϕ CDM), and the intrinsic scatter σ_{int} ranges from a high of $0.733^{+0.031}_{-0.596}$ (non-flat XCDM) to a low of $0.589^{+0.023}_{-0.455}$ (non-flat ϕ CDM), with central values of each pair being 0.06σ , 0.54σ , and 0.05σ away from each other, respectively.⁸

In the GL case (with subscript “GL” in the first line of Tables 4, 5, 7, and 8), the slope k ranges from a high of $-1.532^{+0.259}_{-0.260}$ (non-flat XCDM) to a low of $-1.720 \pm$

⁸ Note, however, that the lower error bars of b and σ_{int} are considerably larger than the upper ones due to cut-off prior ranges of the former and skewed distributions of the latter. Therefore here we also consider the MS case with wider prior range of $b \in [-10, 10]$, which are not listed in the tables due to their insignificant differences. Because the lowest and highest values of k , b , and σ_{int} from these two MS cases differ from each other at only 0.22σ , 0.56σ , and 0.37σ , respectively, and the constraints of the cosmological parameters are also within 1σ range, the prior range of $b \in [0, 10]$ is an acceptable choice.

0.219 (flat Λ CDM), the intercept b ranges from a high of $0.556^{+0.127}_{-0.256}$ (flat XCDM) to a low of $0.407^{+0.136}_{-0.160}$ (non-flat Λ CDM), and the intrinsic scatter σ_{int} ranges from a high of $0.429^{+0.059}_{-0.094}$ (flat Λ CDM) to a low of $0.402^{+0.057}_{-0.090}$ (non-flat ϕ CDM), with central values of each pair being 0.55σ , 0.51σ , and 0.25σ away from each other, respectively.

Figure 1, panel (c), shows that the GL and MS GRBs obey the same Dainotti correlation in the flat Λ CDM model, within the uncertainties.⁹ Table 6 shows that the differences between the GL and MS Dainotti parameters in all six cosmological models are within 1σ . GL and MS GRBs however follow a different Dainotti correlation than the ML GRBs. Given the similarity of the GL and MS Dainotti

⁹ It is unclear if this is more than just a coincidence, as the plateau phases in the two cases are dominated by GW emission (GL) and MD radiation (MS), respectively.

correlation parameters, it is not unreasonable to use just three (not six) correlation parameters in joint analyses of MS and GL data (with subscript “MS+GL” in the first line of Tables 4 and 5). In this case, the slope k ranges from a high of -1.363 ± 0.175 (non-flat XCDM) to a low of -1.577 ± 0.155 (flat Λ CDM), the intercept b ranges from a high of $0.470^{+0.108}_{-0.206}$ (flat XCDM) to a low of $0.337^{+0.110}_{-0.127}$ (non-flat Λ CDM), and the intrinsic scatter σ_{int} ranges from a high of $0.412^{+0.052}_{-0.079}$ (flat Λ CDM) to a low of $0.357^{+0.046}_{-0.070}$ (non-flat Λ CDM), with central values of each pair being 0.92σ , 0.57σ , and 0.60σ away from each other, respectively. In contrast to the GL case, the MS + GL case tightens the constraints a little bit, with smaller error bars, and prefers lower values of b and σ_{int} , and higher values of k . When we jointly analyze ML + GL and ML + MS, the constraints on the Dainotti parameters follow the same pattern as that of MS + GL against GL.

The constraints on the cosmological parameters are very loose for all of these cases. In the flat Λ CDM model, the highest 2σ lower limit of Ω_{m0} among these cases is $\Omega_{m0} > 0.294$ of the ML + GL data. In the non-flat Λ CDM model, the highest 2σ lower limit of Ω_{m0} is $\Omega_{m0} > 0.391$ of the MS + GL case, which is inconsistent with that of the $H(z)$ + BAO case. The MS data favor open hypersurfaces while all other cases favor closed hypersurfaces, with the favored spatial geometries for GL, ML + GL, and MS + GL data being more than 1σ (or even 2σ) away from flat geometry. In the flat XCDM parametrization, the highest 2σ lower limit of Ω_{m0} is $\Omega_{m0} > 0.192$ for the MS + GL data, and the constraints on the X-fluid equation of state parameter w_X are very loose, with the highest 1σ upper limit being 0.111 for the ML case. In the non-flat XCDM parametrization, the highest 2σ lower limit of Ω_{m0} is $\Omega_{m0} > 0.268$ for the MS + GL data, and the constraints on w_X are very loose, with the highest 1σ upper limit being 0.238 for the MS + GL data. The favored spatial geometries for these cases follow the same pattern as that for non-flat Λ CDM, but with larger upper limits of Ω_{k0} except for the MS data. In the flat ϕ CDM model, the highest 2σ lower limit of Ω_{m0} is $\Omega_{m0} > 0.235$ for the ML + GL data. In the non-flat ϕ CDM model, the highest 2σ lower limit of Ω_{m0} is $\Omega_{m0} > 0.340$ for the ML + GL case, which is inconsistent with that of the $H(z)$ + BAO data. Except for the MS case, closed spatial hypersurfaces are favored, but only in the ML + GL case is flat geometry slightly more than 1σ away. There are no constraints on α from these GRB data.

In the Λ CDM and XCDM cases, all GRB data combinations more favor currently accelerating cosmological expansion. They however more favor currently decelerating cosmological expansion in the ϕ CDM models, in the $\Omega_{m0} - \alpha$ and $\Omega_{m0} - \Omega_{k0}$ parameter subspaces.

From the AIC and BIC values we compute ΔAIC and ΔBIC values with respect to the flat Λ CDM model. These are listed in the last two columns of Table 4. In the ML case, flat Λ CDM is the most favored model but there is only weak or positive evidence against any other model. In the MS case non-flat Λ CDM model is the most favored model and, except for non-flat XCDM (with positive evidence against it), the other models are very strongly disfavored. In the GL case, non-flat Λ CDM is again the most favored model, while the evidence against the others are mostly positive, except for non-flat ϕ CDM (with strong BIC evidence against it). In

Table 6. MD-SGRB and GW-LGRB data $L_0 - t_b$ correlation parameters (and σ_{int}) differences.

Model	$\Delta\sigma_{\text{int}}$	Δk	Δb
Flat Λ CDM	0.48σ	0.31σ	0.80σ
Non-flat Λ CDM	0.50σ	0.31σ	0.01σ
Flat XCDM	0.49σ	0.79σ	0.22σ
Non-flat XCDM	0.55σ	0.26σ	0.07σ
Flat ϕ CDM	0.37σ	0.92σ	0.59σ
Non-flat ϕ CDM	0.36σ	0.87σ	0.36σ

the MS + GL case, similar to the MS case, non-flat Λ CDM is the most favored model and, except for non-flat XCDM (with weak AIC and positive BIC evidence against it), the others are strongly disfavored. In the ML + GL case, non-flat Λ CDM is the most favored model but, except for flat XCDM (with strong BIC evidence against it), the evidence against the other models is either weak or positive. In the ML + MS case, the best candidates are non-flat XCDM based on AIC and flat Λ CDM based on BIC , while the evidence against the other models is either weak or positive.

5.2 Constraints from A118, A115 (and jointly with ML), and A115' (and jointly with GL) data

The A118 data set was previously studied by Khadka et al. (2021b). Here we analyze it along with the truncated A115 and A115' data sets, which are also used in joint analyses with the ML and GL data sets. The constraints from these data sets on the GRB correlation parameters and on the cosmological model parameters are presented in Tables 7 and 8. The corresponding posterior 1D probability distributions and 2D confidence regions of these parameters are shown in Figs. 5 and 6, in gray (A118), red (A115 and A115'), green (ML and GL), and purple (ML + A115 and GL + A115'). Note that these analyses assume $H_0 = 70 \text{ km s}^{-1} \text{ Mpc}^{-1}$ and $\Omega_b = 0.05$.

The constraints from A115 data and from ML data, and from A115' data and from GL data, are not mutually inconsistent, so it is not unreasonable to examine joint ML + A115 and GL + A115' constraints. The ML data have the smallest intrinsic dispersion, $\sim 0.30 - 0.31$, with A115, A115', and GL having larger intrinsic dispersion, $\sim 0.40 - 0.43$.

The constraints on the Amati parameters are quite cosmological-model-independent for these GRB data sets. In the A118 case, the slope β ranges from a high of 1.121 ± 0.091 (non-flat XCDM) to a low of 1.106 ± 0.089 (flat XCDM), the intercept γ ranges from a high of $50.15^{+0.26}_{-0.30}$ (flat XCDM) to a low of 50.01 ± 0.26 (non-flat Λ CDM), and the intrinsic scatter σ_{int} ranges from a high of $0.412^{+0.028}_{-0.034}$ (flat XCDM) to a low of $0.411^{+0.027}_{-0.033}$ (flat ϕ CDM), with central values of each pair being 0.12σ , 0.35σ , and 0.02σ away from each other, respectively.

In the A115 case, the slope β ranges from a high of 1.124 ± 0.092 (non-flat Λ CDM) to a low of 1.109 ± 0.092 (flat XCDM), the intercept γ ranges from a high of $50.14^{+0.27}_{-0.31}$ (flat XCDM) to a low of 50.00 ± 0.27 (non-flat Λ CDM), and the intrinsic scatter σ_{int} ranges from a high of $0.418^{+0.028}_{-0.034}$ (non-flat XCDM) to a low of $0.416^{+0.028}_{-0.034}$ (flat ϕ CDM), with

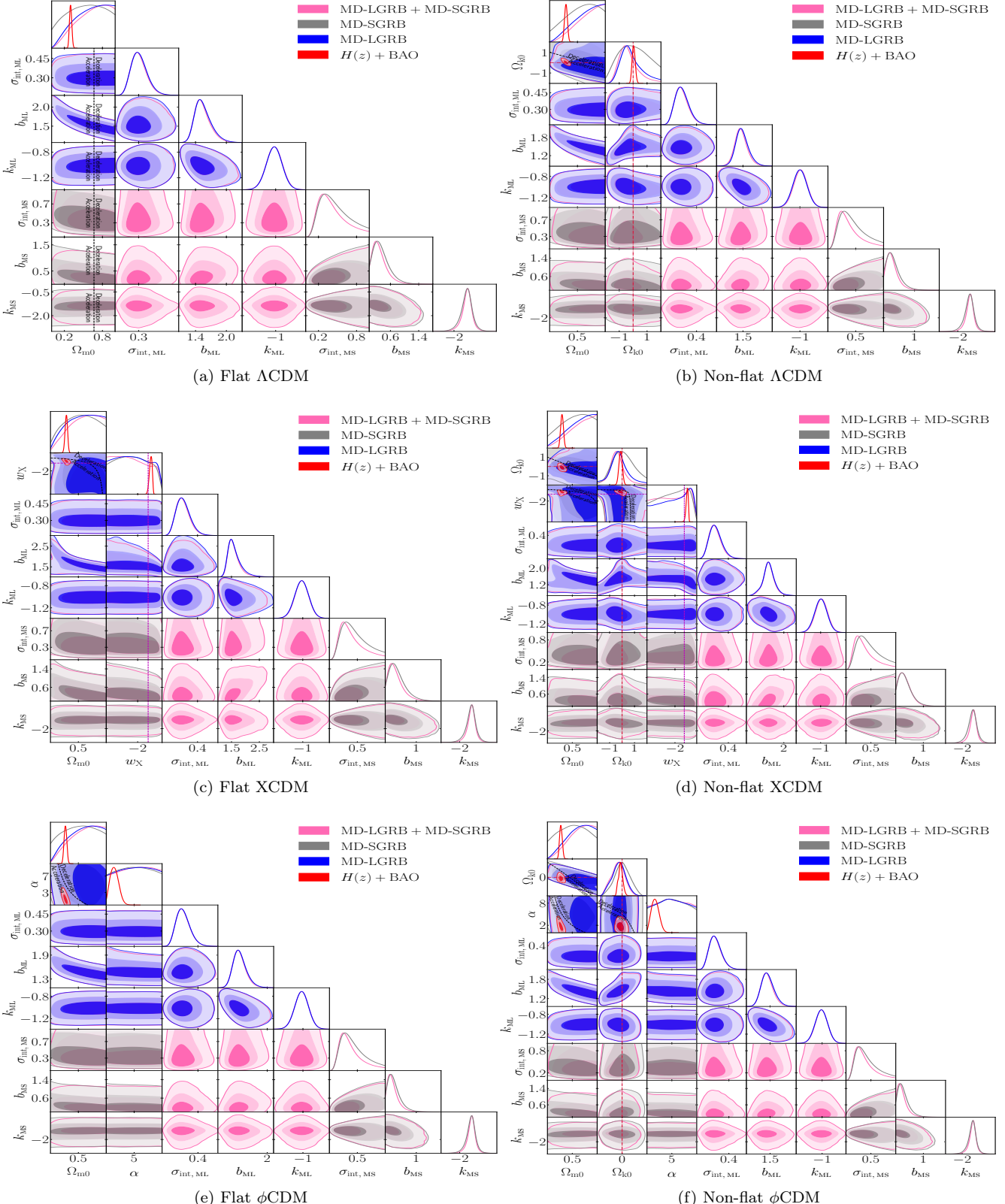


Figure 2. One-dimensional likelihoods and 1σ , 2σ , and 3σ two-dimensional likelihood confidence contours from MD-LGRB (blue), MD-SGRB (gray), MD-LGRB + MD-SGRB (pink), and $H(z)$ + BAO (red) data for all six models. The zero-acceleration lines are shown as black dashed lines, which divide the parameter space into regions associated with currently-accelerating and currently-decelerating cosmological expansion. In the non-flat XCDM and non-flat ϕ CDM cases, the zero-acceleration lines are computed for the third cosmological parameter set to the $H(z)$ + BAO data best-fitting values listed in Table 4. The crimson dash-dot lines represent flat hypersurfaces, with closed spatial hypersurfaces either below or to the left. The magenta lines represent $w_X = -1$, i.e. flat or non-flat Λ CDM models. The $\alpha = 0$ axes correspond to flat and non-flat Λ CDM models in panels (e) and (f), respectively.

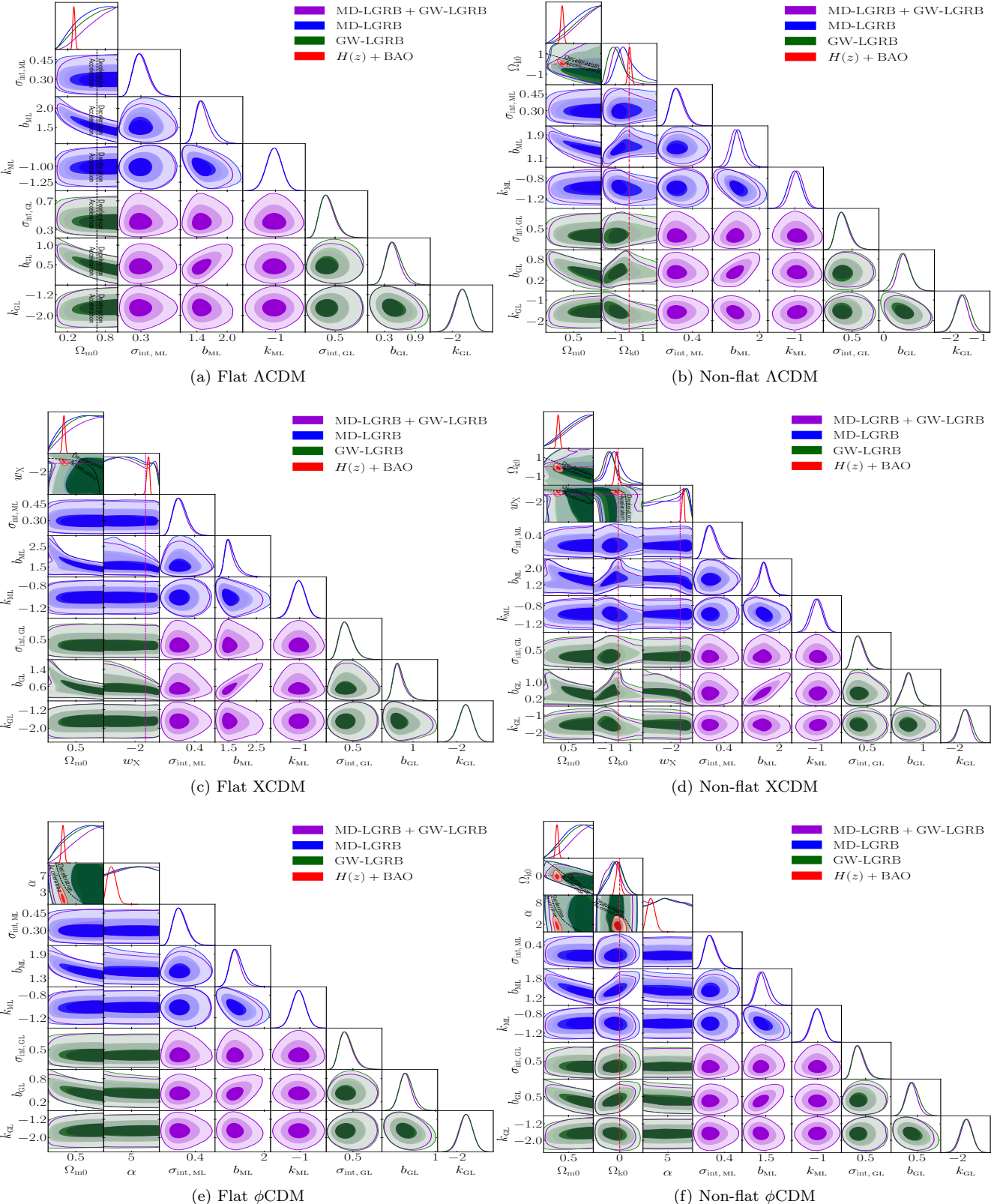


Figure 3. One-dimensional likelihoods and 1σ , 2σ , and 3σ two-dimensional likelihood confidence contours from MD-LGRB (blue), GW-LGRB (green), MD-LGRB + GW-LGRB (violet), and $H(z) + \text{BAO}$ (red) data for all six models. The zero-acceleration lines are shown as black dashed lines, which divide the parameter space into regions associated with currently-accelerating and currently-decelerating cosmological expansion. In the non-flat XCDM and non-flat ϕ CDM cases, the zero-acceleration lines are computed for the third cosmological parameter set to the $H(z) + \text{BAO}$ data best-fitting values listed in Table 4. The crimson dash-dot lines represent flat hypersurfaces, with closed spatial hypersurfaces either below or to the left. The magenta lines represent $w_X = -1$, i.e. flat or non-flat Λ CDM models. The $\alpha = 0$ axes correspond to flat and non-flat Λ CDM models in panels (e) and (f), respectively.

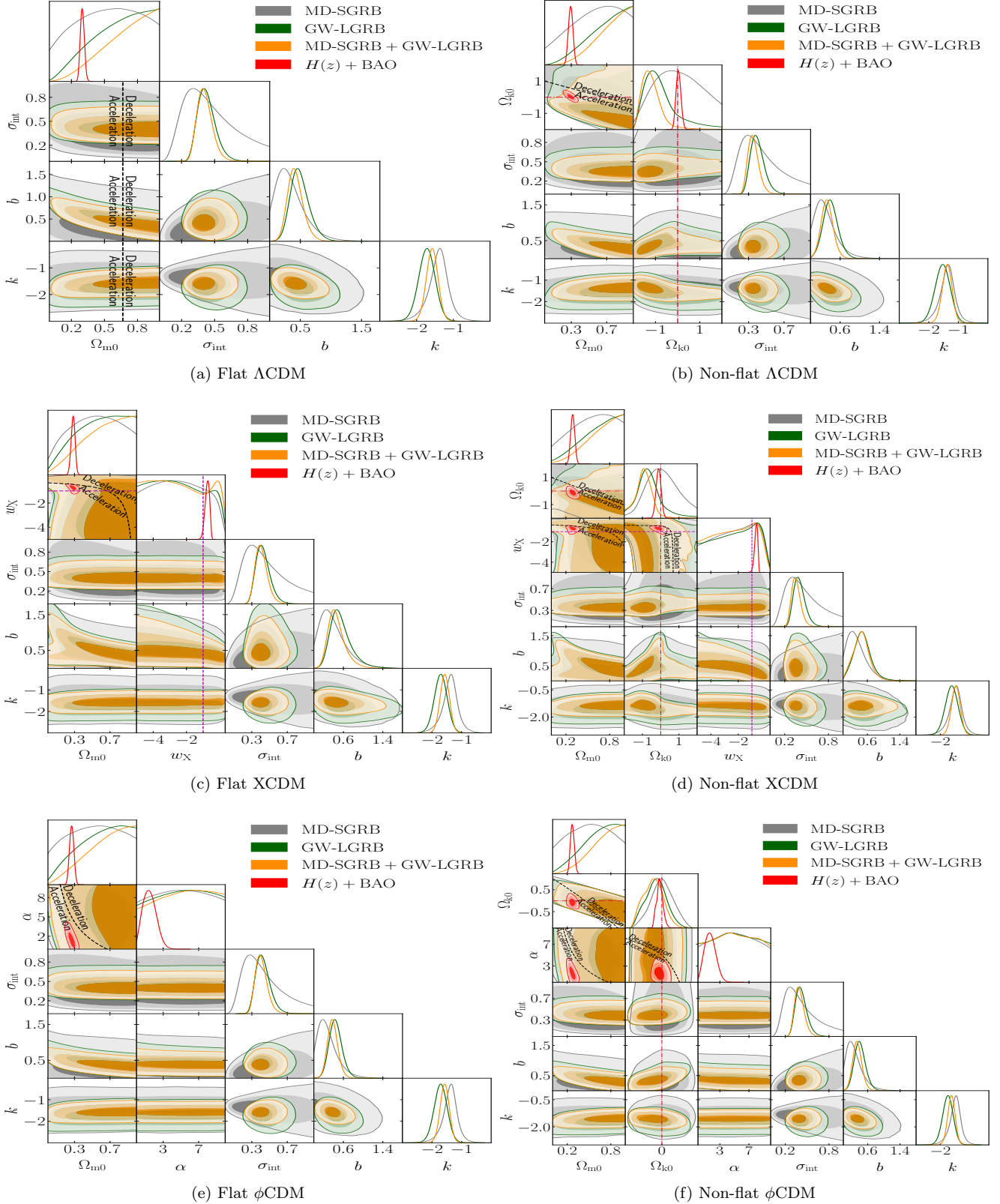


Figure 4. One-dimensional likelihoods and 1σ , 2σ , and 3σ two-dimensional likelihood confidence contours from MD-SGRB (gray), GW-LGRB (green), MD-SGRB + GW-LGRB (orange), and $H(z) + \text{BAO}$ (red) data for all six models, without subscripts on σ_{int} , k , and b . The zero-acceleration lines are shown as black dashed lines, which divide the parameter space into regions associated with currently-accelerating and currently-decelerating cosmological expansion. In the non-flat XCDM and non-flat ϕ CDM cases, the zero-acceleration lines are computed for the third cosmological parameter set to the $H(z) + \text{BAO}$ data best-fitting values listed in Table 4. The crimson dash-dot lines represent flat hypersurfaces, with closed spatial hypersurfaces either below or to the left. The magenta lines represent $w_X = -1$, i.e. flat or non-flat Λ CDM models. The $\alpha = 0$ axes correspond to flat and non-flat Λ CDM models in panels (e) and (f), respectively.

Table 7: Unmarginalized best-fitting parameter values for all models from various combinations of data.^a

Model	Data set	$\Omega_c h^2$	$\Omega_{\text{m}0}$	w_{X}	α	$\sigma_{\text{int, ML}}$	b_{ML}	k_{ML}	σ_{int}	γ	β	$\sigma_{\text{int, cl}}$	b_{cl}	k_{cl}	$-2 \ln \mathcal{L}_{\text{max}}$	AIC	BIC	ΔAIC	ΔBIC			
Flat Λ CDM	A118	0.4089	0.884	—	—	—	0.275	1.383	-1.010	—	0.401	50.02	1.099	—	—	128.72	136.72	147.81	0.00	0.00		
	ML	0.4645	0.998	—	—	—	—	—	—	—	0.405	50.01	1.099	—	—	8.68	16.68	22.41	0.00	0.00		
	A115	0.4172	0.901	—	—	—	0.274	1.400	-1.019	0.407	50.00	1.097	—	—	—	127.97	135.97	146.95	0.00	0.00		
	ML + A115	0.4540	0.977	—	—	—	—	—	—	—	0.403	50.01	1.091	—	—	136.70	150.70	171.59	0.00	0.00		
	GL	0.4641	0.997	—	—	—	—	—	—	—	0.402	49.96	1.110	0.370	0.359	-1.675	22.94	30.94	35.65	0.00	0.00	
	A115'	0.4629	0.995	—	—	—	—	—	—	—	0.402	49.96	1.110	0.370	0.363	-1.666	126.34	134.34	145.32	0.00	0.00	
Non-flat Λ CDM	A118	0.4622	0.993	0.907	—	—	—	—	—	—	0.400	49.92	1.115	—	—	—	127.96	137.96	151.82	1.24	4.01	
	ML	0.4410	0.950	-0.973	—	—	0.268	1.316	-0.967	—	0.403	49.90	1.118	—	—	—	7.48	17.48	24.65	0.80	2.24	
	A115	0.4631	0.955	1.014	—	—	—	—	—	—	0.400	50.01	1.088	—	—	—	127.18	137.18	150.90	1.21	3.95	
	ML + A115	0.4637	0.996	0.062	—	—	0.283	1.383	-1.006	—	0.410	50.01	1.088	—	—	—	136.74	152.74	176.61	2.04	5.02	
	GL	0.4640	0.997	-1.703	—	—	—	—	—	—	0.404	49.94	1.110	—	0.239	0.238	-1.377	17.00	27.00	32.89	-3.94	
	A115'	0.4647	0.998	0.729	—	—	—	—	—	—	0.402	50.00	1.100	0.362	0.364	-1.674	125.93	135.93	149.65	1.59	4.33	
Flat XCDM	A118	-0.0115	0.027	—	-0.098	—	-0.275	1.288	-0.997	—	0.399	50.04	1.102	—	—	—	128.43	138.43	152.29	1.71	4.48	
	ML	0.0327	0.117	—	0.133	—	-0.102	—	-0.102	—	0.407	50.01	1.115	—	—	—	8.14	18.14	25.31	1.46	2.90	
	A115	-0.0197	0.010	—	-4.386	—	-0.273	1.431	-1.008	0.403	50.05	1.093	—	—	—	127.66	137.66	151.38	1.69	4.43		
	ML + A115	0.4065	0.880	—	0.139	—	—	—	—	—	0.402	50.03	1.100	0.364	0.259	-1.651	136.70	152.70	176.57	2.00	4.98	
	GL	0.0035	0.057	—	-0.082	—	—	—	—	—	0.401	49.98	1.084	0.376	0.330	-1.672	21.97	31.97	37.86	1.03	2.21	
	A115'	0.0119	0.074	—	0.122	—	—	—	—	—	0.401	49.98	1.084	0.376	0.330	-1.672	126.22	136.22	149.94	1.88	4.62	
Non-flat XCDM	A118	0.2817	0.625	—	—	—	—	—	—	—	0.399	49.98	1.084	—	—	—	149.21	165.21	188.69	1.87	4.81	
	ML	0.4603	0.989	0.841	-1.048	—	0.269	0.949	-0.976	—	0.399	49.93	1.112	—	—	—	127.99	139.99	156.61	3.27	8.80	
	A115	0.1525	0.361	-1.893	0.036	—	0.269	0.949	-0.976	—	0.404	49.91	1.115	—	—	—	7.39	19.39	27.99	2.71	5.58	
	ML + A115	0.4602	0.989	0.955	-1.097	—	0.269	1.478	-1.015	0.404	50.05	1.107	—	—	—	127.18	139.18	155.65	3.21	8.70		
	GL	0.3647	0.794	0.002	-4.000	—	—	—	—	—	0.403	49.94	1.112	—	0.327	0.237	-1.299	16.61	28.61	35.68	4.05	10.01
	A115'	0.0378	0.127	-0.174	-4.518	—	—	—	—	—	0.401	50.03	1.063	0.358	0.296	-1.616	125.92	137.92	154.39	3.58	9.07	
Flat ϕ CDM	A118	0.4349	0.938	-0.255	-0.043	—	—	—	—	—	0.401	49.98	1.084	0.376	0.330	-1.672	149.16	167.16	193.57	3.82	9.69	
	ML	0.2391	0.520	—	—	—	9.936	—	—	—	0.402	50.02	1.109	—	—	—	128.56	138.56	152.41	1.84	4.60	
	A115	0.4651	0.999	—	5.225	0.275	1.383	-1.011	—	—	0.405	50.04	1.106	—	—	—	8.68	18.68	25.85	2.00	3.44	
	ML + A115	0.2065	0.471	—	9.932	—	—	-1.021	0.405	49.99	1.099	—	—	0.372	0.360	-1.674	127.79	137.79	151.52	1.82	4.57	
	GL	0.4563	0.981	—	2.762	0.273	1.391	—	—	—	0.402	50.02	1.096	0.372	0.348	-1.663	136.70	152.70	176.57	2.00	4.98	
	A115'	0.4641	0.997	—	4.299	—	—	—	—	—	0.403	49.94	1.112	—	—	—	22.94	32.94	38.83	2.00	3.18	
Non-flat ϕ CDM	A118	0.3245	0.712	0.245	—	8.862	—	—	0.400	50.01	1.116	—	—	—	—	128.42	140.42	157.04	3.70	9.23		
	ML	0.4558	0.980	-0.980	0.423	0.266	1.296	-0.973	—	—	0.406	50.05	1.108	—	—	—	7.48	19.48	28.09	2.80	5.68	
	A115	0.3217	0.706	0.290	3.150	—	—	-1.001	0.404	50.03	1.095	—	—	—	—	127.64	139.64	156.11	3.67	9.16		
	ML + A115	0.3044	0.671	-0.076	8.893	0.274	1.406	-1.001	—	—	0.404	50.02	1.105	—	0.340	0.337	-1.547	20.15	32.15	39.22	4.07	10.03
	GL	0.4644	0.998	-0.993	0.173	—	—	—	—	—	0.404	50.02	1.105	—	—	—	126.21	138.21	154.68	3.57	9.36	
	A115'	0.3787	0.823	0.161	7.940	—	—	—	—	—	0.400	50.00	1.077	0.372	0.310	-1.622	149.18	167.18	193.59	3.84	9.71	

^a In these GRB cases, Ω_b and H_0 are set to be 0.05 and 70 km s⁻¹ Mpc⁻¹, respectively.

Table 8: One-dimensional marginalized posterior mean values and uncertainties ($\pm 1\sigma$ error bars or 2σ limits) of the parameters for all models from various combinations of data.^a

Model	Data set	Ω_{m0}	Ω_{k0}	w_X	α	$\sigma_{\text{int}, \text{ul}}$	b_{ul}	k_{ul}	σ_{int}	γ	β	$\sigma_{\text{int}, \text{cl}}$	b_{ul}	k_{ul}	
Flat Λ CDM	A118	> 0.247	-	-	-	-	-	-	-	-	-	-	-	-	
	ML	> 0.188	-	-	-	-	0.305 ^{+0.035} _{-0.033}	1.552 ^{+0.108} _{-0.189}	-1.017 \pm 0.090	-	0.412 ^{+0.027} _{-0.033}	5.09 \pm 0.26	1.110 \pm 0.090	-	
	A115	0.630 ^{+0.352} _{-0.135}	-	-	-	-	0.301 ^{+0.033} _{-0.051}	1.515 ^{+0.101} _{-0.151}	-1.015 \pm 0.088	-	0.417 ^{+0.028} _{-0.034}	5.09 \pm 0.26	1.112 \pm 0.093	-	
	ML + A115	> 0.298	-	-	-	-	-	-	-	-	5.07 \pm 0.25	1.111 \pm 0.089	-	-	
	GL	> 0.202	-	-	-	-	-	-	-	-	-	0.429 ^{+0.059} _{-0.094}	0.495 ^{+0.120} _{-0.173}	-1.720 \pm 0.219	
	A115'	> 0.264	-	-	-	-	-	-	-	-	-	-	-	-	
Non-flat Λ CDM	ML + A115	> 0.346	-	-	-	-	-	-	-	-	-	-	-	-	
	GL	> 0.290	-0.762 ^{+0.211} _{-0.830}	-	-	-	-	-	-	-	-	-	-	-	
	A115	> 0.299	0.599 ^{+0.582} _{-0.887}	-	-	-	-	-	-	-	-	-	-	-	
	A115'	> 0.381	0.214 ^{+0.228} _{-0.855}	-	-	-	-	-	-	-	-	-	-	-	
	GL + A115'	-	-	-	-	-	-	-	-	-	-	-	-	-	
	A118	0.599 ^{+0.350} _{-0.175}	-	-2.440 ^{+1.779} _{-2.456^{+2.367}_{-2.369}}	-	-	-	-	-1.014 \pm 0.092	-	0.412 ^{+0.028} _{-0.034}	5.015 ^{+0.26} _{-0.30}	1.106 \pm 0.089	-	
Flat XCDM	ML	> 0.123	-	-2.411 ^{+2.760} _{-1.729}	-	-	-	-	-	-	-	-	-	-	
	A115	0.589 ^{+0.357} _{-0.184}	-	< -0.041	-	-	-	-	-1.012 \pm 0.088	-	0.417 ^{+0.028} _{-0.034}	5.014 ^{+0.27} _{-0.31}	1.109 \pm 0.092	-	
	ML + A115	> 0.191	-	< -0.046	-	-	-	-	-	-	5.03 \pm 0.26	1.108 \pm 0.090	-	-	
	GL	> 0.141	-	-	-	-	-	-	-	-	-	0.428 ^{+0.058} _{-0.092}	0.556 ^{+0.127} _{-0.236}	-1.706 \pm 0.215	
	A115	0.605 ^{+0.394} _{-0.126}	-	-	-	-	-	-	-	-	-	-	-	-	
	GL + A115'	> 0.295	-	< -0.017	-	-	-	-	-	-	-	-	-	-	
Non-flat XCDM	A118	> 0.246	0.590 ^{+0.476} _{-0.796}	-	-	-	-	-	-	-	-	-	-	-	
	ML	> 0.174	-0.262 ^{+0.580} _{-0.244}	-	-2.000 ^{+2.117} _{-2.129}	-	-	0.305 ^{+0.036} _{-0.054}	1.462 ^{+0.194} _{-0.196}	-0.996 \pm 0.097	-	0.412 ^{+0.027} _{-0.033}	5.014 ^{+0.27} _{-0.31}	1.121 \pm 0.091	-
	A115	> 0.240	0.563 ^{+0.498} _{-0.296}	-	-2.290 ^{+2.266} _{-2.796}	-	-	0.300 ^{+0.033} _{-0.051}	1.562 ^{+0.103} _{-0.220}	-1.012 \pm 0.088	-	5.013 ^{+0.27} _{-0.30}	1.108 \pm 0.090	-	-
	ML + A115	> 0.231	0.292 ^{+0.376} _{-0.635}	-	-2.155 ^{+2.224} _{-1.635}	-	-	0.302 ^{+0.033} _{-0.051}	1.489 ^{+0.122} _{-0.167}	-1.016 \pm 0.089	-	0.414 ^{+0.028} _{-0.034}	5.015 ^{+0.27} _{-0.30}	1.103 \pm 0.092	-
	GL	> 0.194	-0.615 ^{+0.470} _{-0.635}	-	-2.212 ^{+2.186} _{-2.186}	-	-	-	-	-	-	0.413 ^{+0.027} _{-0.034}	5.014 ^{+0.26} _{-0.30}	1.101 \pm 0.088	-
	A115'	> 0.236	0.451 ^{+0.485} _{-0.789}	-	-2.210 ^{+2.208} _{-2.946}	-	-	-	-	-	-	0.421 ^{+0.055} _{-0.088}	0.512 ^{+0.113} _{-0.210}	-1.698 \pm 0.208	
Flat ϕ CDM	GL + A115'	> 0.226	0.014 ^{+0.408} _{-0.604}	-	-2.080 ^{+2.201} _{-1.138}	-	-	-	-	-	-	-	-	-	
	A118	0.568 ^{+0.332} _{-0.230}	-	-	-	-	-	-	-	-	-	-	-	-	
	ML	> 0.148	-	-	-	-	-	-	-	-	-	-	-	-	
	A115	0.365 ^{+0.339} _{-0.228}	-	-	-	-	-	-	-	-	-	-	-	-	
	ML + A115	> 0.198	-	-	-	-	-	-	-	-	-	-	-	-	
	GL	> 0.148	-	-	-	-	-	-	-	-	-	-	-	-	
Non-flat ϕ CDM	A115'	0.386 ^{+0.391} _{-0.156}	-	-	-	-	-	-	-	-	-	-	-	-	
	GL + A115'	> 0.231	-	-	-	-	-	-	-	-	-	-	-	-	
	A118	0.560 ^{+0.256} _{-0.207}	-	-	-	-	-	-	-	-	-	-	-	-	
	ML	> 0.163 ^{+0.355} _{-0.317}	-	-	-	-	-	-	-	-	-	-	-	-	
	A115	0.546 ^{+0.260} _{-0.293}	0.011 ^{+0.293} _{-0.181}	-	-	-	-	-	-	-	-	-	-	-	
	ML + A115	0.630 ^{+0.286} _{-0.286}	-0.108 ^{+0.296} _{-0.263}	-	-	-	-	-	-	-	-	-	-	-	
Non-flat ϕ CDM	GL	> 0.207	-0.193 ^{+0.364} _{-0.187}	-	-	-	-	-	-	-	-	-	-	-	
	A115'	0.381 ^{+0.254} _{-0.237}	-0.033 ^{+0.296} _{-0.290}	-	-	-	-	-	-	-	-	-	-	-	
	GL + A115'	0.666 ^{+0.327} _{-0.166}	-0.169 ^{+0.317} _{-0.270}	-	-	-	-	-	-	-	-	-	-	-	

^a In these GRB cases, Ω_b and H_0 are set to be 0.05 and 70 km s⁻¹ Mpc⁻¹, respectively.

central values of each pair being 0.12σ , 0.34σ , and 0.05σ away from each other, respectively.

In the A115' case, the slope β ranges from a high of 1.117 ± 0.090 (non-flat Λ CDM) to a low of 1.103 ± 0.092 (flat XCDM), the intercept γ ranges from a high of $50.15^{+0.27}_{-0.30}$ (flat XCDM) to a low of 50.02 ± 0.26 (non-flat Λ CDM), and the intrinsic scatter σ_{int} ranges from a high of $0.415^{+0.028}_{-0.034}$ (non-flat XCDM) to a low of $0.414^{+0.028}_{-0.034}$ (the others), with central values of each pair being 0.11σ , 0.33σ , and 0.02σ away from each other, respectively.

The lowest and highest values of β , γ , and σ_{int} from the A118, A115, and A115' cases differ from each other at 0.16σ , 0.37σ , and 0.16σ , respectively. This implies that excluding three GRBs from A118 does not significantly affect the constraints on the Amati parameters.

In the joint analysis of ML and A115 (ML + A115) data, β ranges from a high of 1.113 ± 0.091 (non-flat Λ CDM) to a low of 1.106 ± 0.090 (non-flat ϕ CDM), γ ranges from a high of $50.13^{+0.27}_{-0.30}$ (flat XCDM) to a low of 50.03 ± 0.25 (flat and non-flat ϕ CDM), and σ_{int} ranges from a high of $0.417^{+0.028}_{-0.034}$ (flat XCDM) to a low of $0.416^{+0.027}_{-0.034}$ (flat Λ CDM, and flat and non-flat ϕ CDM), with central values of each pair being 0.05σ , 0.26σ , and 0.02σ away from each other, respectively; also k ranges from a high of -1.012 ± 0.088 (flat XCDM) to a low of -1.019 ± 0.091 (non-flat Λ CDM), b ranges from a high of $1.562^{+0.103}_{-0.220}$ (flat XCDM) to a low of $1.453^{+0.115}_{-0.139}$ (non-flat ϕ CDM), and $\sigma_{\text{int, ML}}$ ranges from a high of $0.304^{+0.034}_{-0.052}$ (non-flat Λ CDM) to a low of $0.300^{+0.033}_{-0.051}$ (flat XCDM), with central values of each pair being 0.06σ , 0.44σ , and 0.06σ away from each other, respectively. The lowest and highest values of β , γ , and σ_{int} from the A115 and ML + A115 cases differ from each other at 0.14σ , 0.32σ , and 0.05σ , respectively; also those of k , b , and $\sigma_{\text{int, ML}}$ differ from each other at 0.17σ , 0.53σ , and 0.09σ , respectively.

In the joint analysis of GL and A115' (GL + A115') data, β ranges from a high of 1.104 ± 0.089 (flat Λ CDM) to a low of 1.096 ± 0.089 (non-flat ϕ CDM), γ ranges from a high of $50.14^{+0.26}_{-0.30}$ (flat XCDM) to a low of 50.04 ± 0.25 (non-flat ϕ CDM), and σ_{int} ranges from a high of $0.415^{+0.027}_{-0.033}$ (non-flat XCDM) to a low of $0.413^{+0.027}_{-0.034}$ (flat Λ CDM, flat XCDM, and non-flat ϕ CDM), with central values of each pair being 0.06σ , 0.26σ , and 0.05σ away from each other, respectively; also k ranges from a high of -1.682 ± 0.208 (non-flat XCDM) to a low of -1.705 ± 0.210 (flat Λ CDM), b ranges from a high of $0.512^{+0.113}_{-0.210}$ (flat XCDM) to a low of $0.401^{+0.115}_{-0.128}$ (non-flat ϕ CDM), and $\sigma_{\text{int, GL}}$ ranges from a high of $0.423^{+0.056}_{-0.090}$ (flat and non-flat Λ CDM) to a low of $0.416^{+0.055}_{-0.088}$ (non-flat XCDM), with central values of each pair being 0.08σ , 0.46σ , and 0.07σ away from each other, respectively. The lowest and highest values of β , γ , and σ_{int} from the A115' and GL + A115' cases differ from each other at 0.17σ , 0.30σ , and 0.05σ , respectively; also those of k , b , and $\sigma_{\text{int, GL}}$ differ from each other at 0.52σ , 0.47σ , and 0.20σ , respectively.

Judging from the constraints on the parameters of the Amati and Dainotti correlations, those from the joint analyses do not deviate much from the individual cases. We next focus on constraints on cosmological model parameters.

Similar to GRB data from Sec. 5.1, these data more favor currently accelerating cosmological expansion in the Λ CDM and XCDM cases, but also more favor currently de-

celerating cosmological expansion in the ϕ CDM models, in the $\Omega_{\text{m}0} - \alpha$ and $\Omega_{\text{m}0} - \Omega_{\text{k}0}$ parameter subspaces.

In the flat Λ CDM model, the A118, A115, and A115' 2σ constraints on $\Omega_{\text{m}0}$ are mutually consistent (A115 with $\Omega_{\text{m}0} > 0.241$), but they favor higher values of $\Omega_{\text{m}0}$ than do ML and GL while the joint ML + A115 and GL + A115' cases favor even higher values of > 0.298 and > 0.339 , respectively. In fact, this is also true for the ML + GL case ($\Omega_{\text{m}0} > 0.294$).

In the non-flat Λ CDM model, the A118, A115, and A115' 2σ constraints on $\Omega_{\text{m}0}$ are also mutually consistent, but they favor slightly higher values of $\Omega_{\text{m}0}$ than in the flat Λ CDM case, with $\Omega_{\text{m}0} > 0.299$ in the A115' non-flat Λ CDM case. The joint ML + A115, GL + A115', and ML + GL cases favor higher $\Omega_{\text{m}0}$ 2σ limits of > 0.346 , > 0.381 , and > 0.338 , respectively. The A118, A115, ML + A115, A115', and GL + A115' data mildly favor open hypersurfaces in the non-flat Λ CDM model, being less than 1σ away from flatness.

In the flat and non-flat XCDM parametrizations, the 2σ constraints on $\Omega_{\text{m}0}$ are mutually consistent in all cases, where in the flat XCDM parametrization, the 2σ limits are $\Omega_{\text{m}0} > 0.181$ (A118), > 0.170 (A115), and > 0.185 (A115'). The constraints on w_X are very loose, and thus affected by the w_X prior, and consistent with each other in all cases, and mildly favor phantom dark energy (but Λ is less than 1σ away). In the non-flat XCDM parametrization, the A118, A115, ML + A115, A115', and GL + A115' data also mildly favor open hypersurfaces, with flatness being less than 1σ away.

In the flat ϕ CDM model, the A118, A115, and A115' constraints on $\Omega_{\text{m}0}$ are mutually consistent, with 2σ limits of $\Omega_{\text{m}0} > 0.149$ (A118), > 0.145 (A115), and > 0.159 (A115'), which are consistent with the other cases. These GRB data do not provide constraints on α in the flat ϕ CDM model, while in the non-flat ϕ CDM model, A118 and A115' provide constraints of $\alpha = 5.203^{+3.808}_{-2.497}$ and $\alpha = 5.215^{+3.853}_{-2.429}$, respectively. Note that $\alpha = 0$ is still within 2σ for both cases. Similar trends hold for non-flat ϕ CDM $\Omega_{\text{m}0}$ constraints, but ML + A115 and GL + A115' data constraints posterior mean values are larger than for the individual data sets. The 2σ limits are $\Omega_{\text{m}0} > 0.183$ (A118), $\Omega_{\text{m}0} = 0.546^{+0.449}_{-0.384}$ (A115), $\Omega_{\text{m}0} > 0.198$ (A115'), > 0.251 (ML + A115), and > 0.286 (GL + A115'). Except for the A115 data, non-flat ϕ CDM constraints favor closed hypersurfaces (unlike non-flat Λ CDM and non-flat XCDM), but with flatness well within 1σ for all cases.

The ΔAIC and ΔBIC values with respect to the flat Λ CDM model are listed in the last two columns of Table 7. In all cases (except for the GL case, which is discussed in Sec. 5.1 above), the flat Λ CDM model is the most favored model but the evidence against the other models are either weak or positive, except that, based on BIC , the evidence against non-flat XCDM and non-flat ϕ CDM are strong. For ML + A115 data the non-flat ϕ CDM model is very strongly disfavored with $\Delta BIC = 10.03$.

In summary, while the joint analyses do slightly tighten the constraints, the improvements relative to those from A118 data alone are not significant.

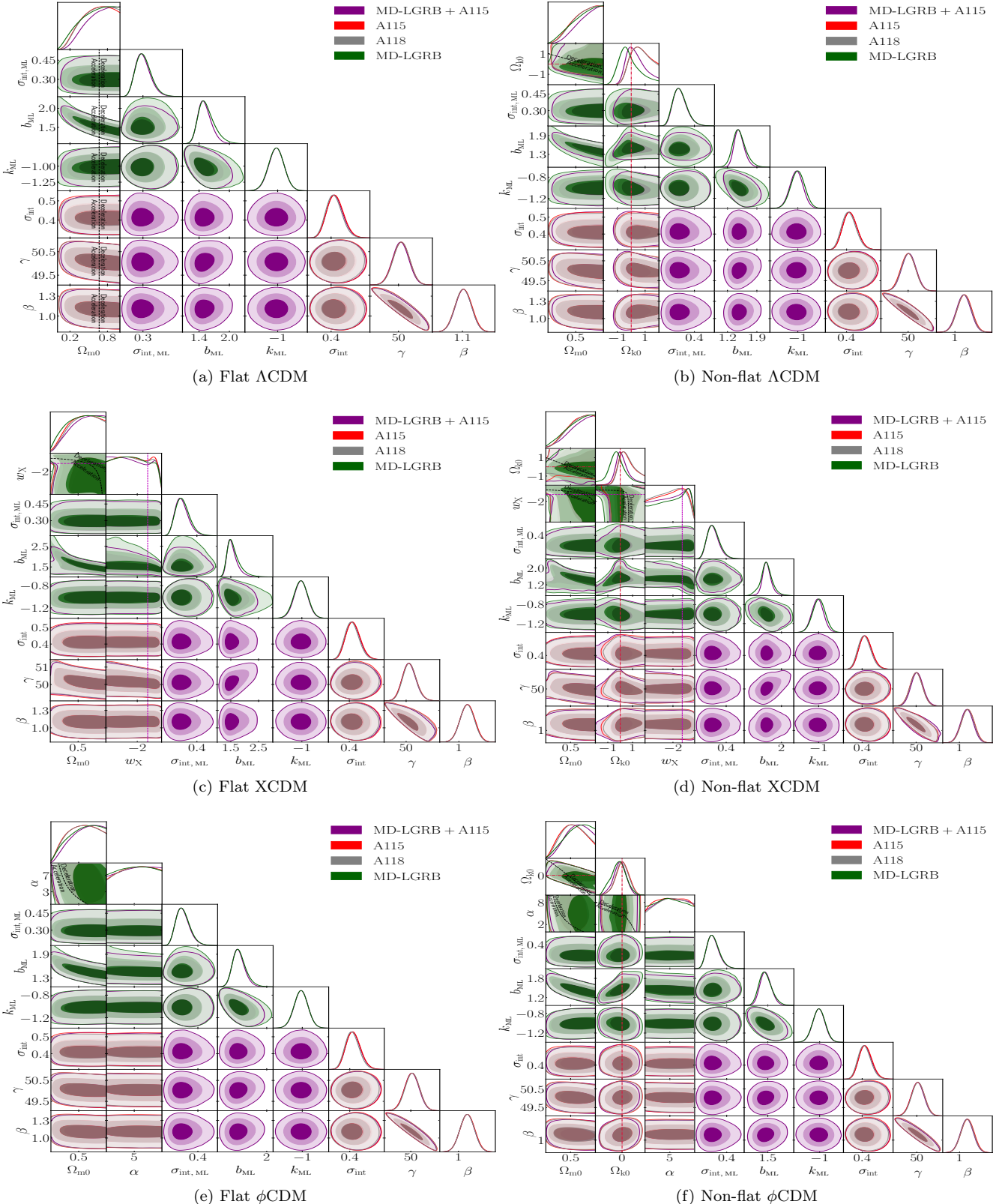


Figure 5. One-dimensional likelihoods and 1σ , 2σ , and 3σ two-dimensional likelihood confidence contours from MD-LGRB (green), A118 (gray), A115 (red), and MD-LGRB + A115 (purple) data for all six models. The zero-acceleration lines are shown as black dashed lines, which divide the parameter space into regions associated with currently-accelerating and currently-decelerating cosmological expansion. In the non-flat XCDM and non-flat ϕ CDM cases, the zero-acceleration lines are computed for the third cosmological parameter set to the $H(z)$ + BAO data best-fitting values listed in Table 7. The crimson dash-dot lines represent flat hypersurfaces, with closed spatial hypersurfaces either below or to the left. The magenta lines represent $w_X = -1$, i.e. flat or non-flat Λ CDM models. The $\alpha = 0$ axes correspond to flat and non-flat Λ CDM models in panels (e) and (f), respectively.

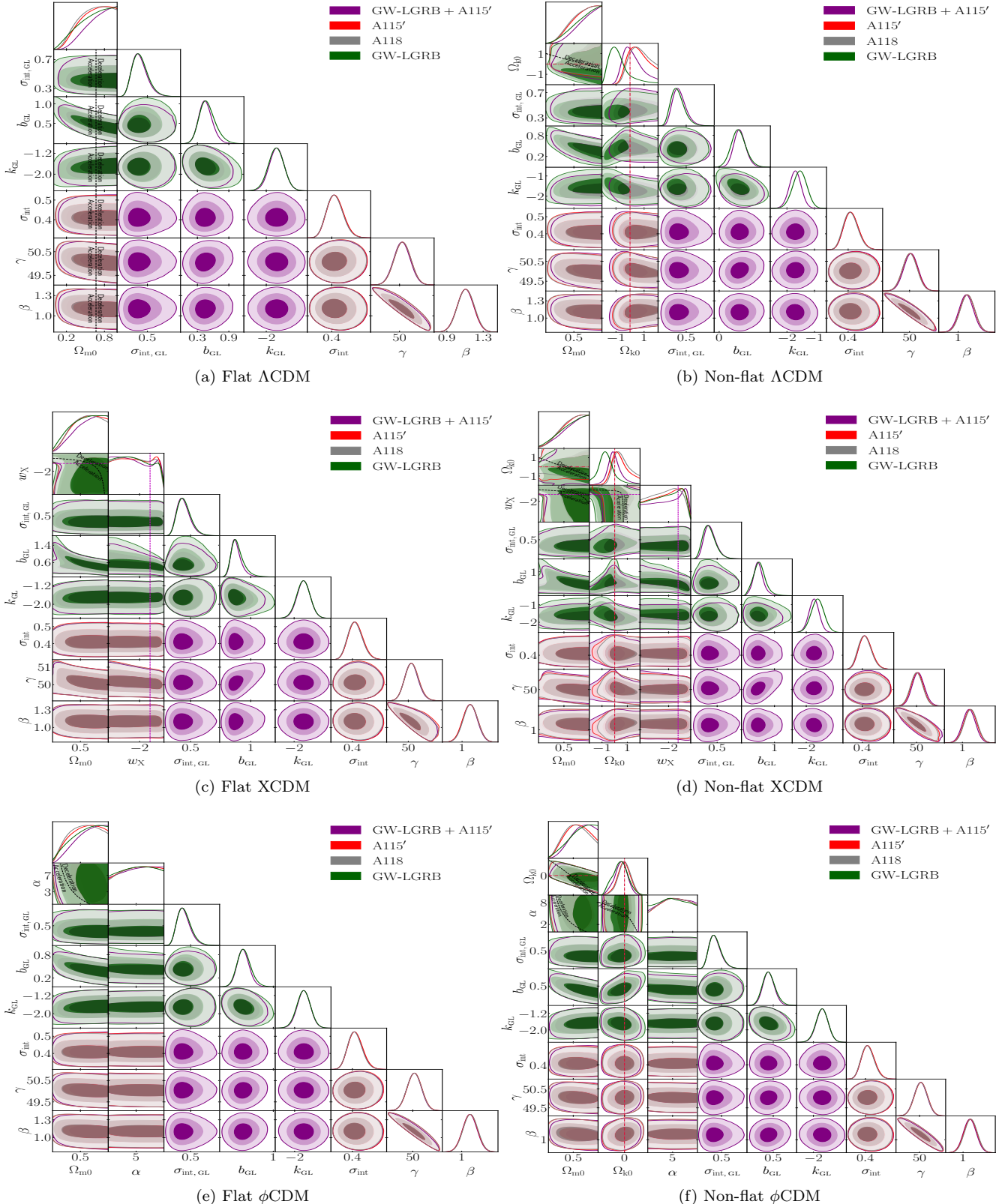


Figure 6. One-dimensional likelihoods and 1 σ , 2 σ , and 3 σ two-dimensional likelihood confidence contours from GW-LGRB (green), A118 (gray), A115' (red), and GW-LGRB + A115' (purple) data for all six models. The zero-acceleration lines are shown as black dashed lines, which divide the parameter space into regions associated with currently-accelerating and currently-decelerating cosmological expansion. In the non-flat XCDM and non-flat ϕ CDM cases, the zero-acceleration lines are computed for the third cosmological parameter set to the $H(z)$ + BAO data best-fitting values listed in Table 7. The crimson dash-dot lines represent flat hypersurfaces, with closed spatial hypersurfaces either below or to the left. The magenta lines represent $w_X = -1$, i.e. flat or non-flat Λ CDM models. The $\alpha = 0$ axes correspond to flat and non-flat Λ CDM models in panels (e) and (f), respectively.

6 CONCLUSION

We have used six different cosmological models in analyses of the three (ML, MS, and GL) Dainotti ($L_0 - t_b$) correlation GRB data sets compiled by Wang et al. (2021) and Hu et al. (2021). We find for each data sets, as well as the MS + GL, ML + GL, and ML + MS combinations, that the GRB correlation parameters are independent of cosmological model. Our results thus indicate that these GRBs are standardizable through the Dainotti correlation and so can be used to constrain cosmological parameters, justifying the assumption made by Wang et al. (2021) and Hu et al. (2021). These results also mean that the circularity problem does not affect cosmological parameter constraints derived from these GRB data.

In contrast to Wang et al. (2021) and Hu et al. (2021) we do not use $H(z)$ data to calibrate these GRB data, instead we use these data to derive GRB only cosmological constraints. We find that ML, MS, GL, MS + GL, ML + GL, and ML + MS GRBs provide only weak restrictions on cosmological parameters.

We have also used the more-restrictive ML and GL Dainotti data sets in joint analyses with the largest available reliable compilation of Amati ($E_p - E_{iso}$) correlation A118 GRB data (Khadka et al. 2021b), but excluding three overlapping GRBs from the A118 data in the joint analyses. While the joint analyses do result in slightly tighter constraints, typically with larger lower limits on $\Omega_m 0$ than those from the ML, GL, or A118 data alone, the improvements relative to the A118 data constraints are not significant.

Current GRB data provide quite weak constraints on cosmological parameters but do favor currently accelerated cosmological expansion in the Λ CDM models and the XCDM parametrizations. We hope that in the near future there will be more and better-quality GRB measurements that will result in more restrictive GRB cosmological constraints. GRBs probe a very wide range of cosmological redshift space, a significant part of which is as yet unprobed, so it is worth putting effort into further developing GRB cosmological constraints.

ACKNOWLEDGEMENTS

We thank F. Y. Wang and J. P. Hu for valuable discussions. This research was supported in part by DOE grant DE-SC0011840. Part of the computation for this project was performed on the Beocat Research Cluster at Kansas State University.

DATA AVAILABILITY

MD-LGRB data are available in Wang et al. (2021) and MD-SGRB and GW-LGRB data are available in Hu et al. (2021).

REFERENCES

- Amati L., Guidorzi C., Frontera F., Della Valle M., Finelli F., Landi R., Montanari E., 2008, *MNRAS*, **391**, 577
 Amati L., Frontera F., Guidorzi C., 2009, *A&A*, **508**, 173
- Amati L., D'Agostino R., Luongo O., Muccino M., Tantalo M., 2019, *MNRAS*, **486**, L46
 Arjona R., Nesseris S., 2021, *Phys. Rev. D*, **103**, 103539
 Brinckmann T., Lesgourgues J., 2019, *Physics of the Dark Universe*, **24**, 100260
 Cao S., Biesiada M., Jackson J., Zheng X., Zhao Y., Zhu Z.-H., 2017, *J. Cosmology Astropart. Phys.*, **2**, 012
 Cao S., Ryan J., Ratra B., 2020, *MNRAS*, **497**, 3191
 Cao S., Ryan J., Ratra B., 2021a, *MNRAS*,
 Cao S., Ryan J., Khadka N., Ratra B., 2021b, *MNRAS*, **501**, 1520
 Cao S., Ryan J., Ratra B., 2021c, *MNRAS*, **504**, 300
 Cardone V. F., Dainotti M. G., Capozziello S., Willingale R., 2010, *MNRAS*, **408**, 1181
 Chávez R., Terlevich R., Terlevich E., Bresolin F., Melnick J., Plionis M., Basilakos S., 2014, *MNRAS*, **442**, 3565
 Chen Y., Ratra B., Biesiada M., Li S., Zhu Z.-H., 2016, *ApJ*, **829**, 61
 Chen Y., Kumar S., Ratra B., 2017, *ApJ*, **835**, 86
 D'Agostini G., 2005, preprint, ([arXiv:physics/0511182](https://arxiv.org/abs/physics/0511182))
 DES Collaboration 2019, *Phys. Rev. D*, **99**, 123505
 Dainotti M. G., Del Vecchio R., 2017, *New Astron. Rev.*, **77**, 23
 Dainotti M. G., Cardone V. F., Capozziello S., 2008, *Monthly Notices of the Royal Astronomical Society: Letters*, **391**, L79
 Dainotti M. G., Willingale R., Capozziello S., Cardone V. F., Ostrowski M., 2010, *The Astrophysical Journal*, **722**, L215
 Dainotti M. G., Cardone V. F., Capozziello S., Ostrowski M., Willingale R., 2011, *The Astrophysical Journal*, **730**, 135
 Dainotti M. G., Cardone V. F., Piedipalumbo E., Capozziello S., 2013a, *MNRAS*, **436**, 82
 Dainotti M. G., Petrosian V., Singal J., Ostrowski M., 2013b, *ApJ*, **774**, 157
 Dainotti M. G., Nagataki S., Maeda K., Postnikov S., Pian E., 2017, *A&A*, **600**, A98
 de Cruz Perez J., Sola Peracaula J., Gomez-Valent A., Moreno-Pulido C., 2021, preprint, ([arXiv:2110.07569](https://arxiv.org/abs/2110.07569))
 Demianski M., Piedipalumbo E., Sawant D., Amati L., 2021, *MNRAS*, **506**, 903
 Dhawan S., Alsing J., Vagnozzi S., 2021, *MNRAS*, **506**, L1
 Di Valentino E., et al., 2021a, *Classical and Quantum Gravity*, **38**, 153001
 Di Valentino E., Melchiorri A., Silk J., 2021b, *ApJ*, **908**, L9
 eBOSS Collaboration 2021, *Phys. Rev. D*, **103**, 083533
 Efstathiou G., Gratton S., 2020, *MNRAS*, **496**, L91
 Fana Dirirsa F., et al., 2019, *ApJ*, **887**, 13
 Farooq O., Ranjeet Madiyar F., Crandall S., Ratra B., 2017, *ApJ*, **835**, 26
 Foreman-Mackey D., Hogg D. W., Lang D., Goodman J., 2013, *PASP*, **125**, 306
 González-Morán A. L., et al., 2019, *MNRAS*, **487**, 4669
 González-Morán A. L., et al., 2021, *MNRAS*,
 Handley W., 2019, *Phys. Rev. D*, **100**, 123517
 Hu J. P., Wang F. Y., Dai Z. G., 2021, *MNRAS*, **507**, 730
 Johnson J. P., Sangwan A., Shankaranarayanan S., 2021, preprint, ([arXiv:2102.12367](https://arxiv.org/abs/2102.12367))
 Khadka N., Ratra B., 2020a, *MNRAS*, **492**, 4456
 Khadka N., Ratra B., 2020b, *MNRAS*, **497**, 263
 Khadka N., Ratra B., 2020c, *MNRAS*, **499**, 391
 Khadka N., Ratra B., 2021a, preprint, ([arXiv:2107.07600](https://arxiv.org/abs/2107.07600))
 Khadka N., Ratra B., 2021b, *MNRAS*, **502**, 6140
 Khadka N., Yu Z., Zajaček M., Martinez-Aldama M. L., Czerny B., Ratra B., 2021a, *MNRAS*, **508**, 4722
 Khadka N., Luongo O., Muccino M., Ratra B., 2021b, *J. Cosmology Astropart. Phys.*, **2021**, 042
 KiDS Collaboration 2021, *A&A*, **649**, A88
 Li E.-K., Du M., Xu L., 2020, *MNRAS*, **491**, 4960
 Li X., Keeley R. E., Shafieloo A., Zheng X., Cao S., Biesiada M., Zhu Z.-H., 2021, *MNRAS*, **507**, 919

- Lian Y., Cao S., Biesiada M., Chen Y., Zhang Y., Guo W., 2021, *MNRAS*, **505**, 2111
- Luongo O., Muccino M., 2021, *Galaxies*, 9
- Luongo O., Muccino M., Colgáin E. Ó., Sheikh-Jabbari M. M., Yin L., 2021, preprint, ([arXiv:2108.13228](#))
- Lusso E., et al., 2020, *A&A*, **642**, A150
- Mania D., Ratra B., 2012, *Physics Letters B*, **715**, 9
- Ooba J., Ratra B., Sugiyama N., 2018a, *ApJ*, **864**, 80
- Ooba J., Ratra B., Sugiyama N., 2018b, *ApJ*, **866**, 68
- Ooba J., Ratra B., Sugiyama N., 2018c, *ApJ*, **869**, 34
- Ooba J., Ratra B., Sugiyama N., 2019, *Ap&SS*, **364**, 176
- Park C.-G., Ratra B., 2018, *ApJ*, **868**, 83
- Park C.-G., Ratra B., 2019a, *Ap&SS*, **364**, 82
- Park C.-G., Ratra B., 2019b, *Ap&SS*, **364**, 134
- Park C.-G., Ratra B., 2019c, *ApJ*, **882**, 158
- Park C.-G., Ratra B., 2020, *Phys. Rev. D*, **101**, 083508
- Pavlov A., Westmoreland S., Saaidi K., Ratra B., 2013, *Phys. Rev. D*, **88**, 123513
- Peebles P. J. E., 1984, *ApJ*, **284**, 439
- Peebles P. J. E., Ratra B., 1988, *ApJ*, **325**, L17
- Perivolaropoulos L., Skara F., 2021, preprint, ([arXiv:2105.05208](#))
- Planck Collaboration 2020, *A&A*, **641**, A6
- Rana A., Jain D., Mahajan S., Mukherjee A., 2017, *J. Cosmology Astropart. Phys.*, **3**, 028
- Ratra B., Peebles P. J. E., 1988, *Phys. Rev. D*, **37**, 3406
- Rezaei M., Peracaula J. S., Malekjani M., 2021, *MNRAS*,
- Risaliti G., Lusso E., 2015, *ApJ*, **815**, 33
- Risaliti G., Lusso E., 2019, *Nature Astronomy*, **3**, 272
- Ryan J., Doshi S., Ratra B., 2018, *MNRAS*, **480**, 759
- Ryan J., Chen Y., Ratra B., 2019, *MNRAS*, **488**, 3844
- Salvaterra R., et al., 2009, *Nature*, **461**, 1258
- Samushia L., Ratra B., 2010, *ApJ*, **714**, 1347
- Sangwan A., Tripathi A., Jassal H. K., 2018, preprint, ([arXiv:1804.09350](#))
- Scolnic D. M., et al., 2018, *ApJ*, **859**, 101
- Singh A., Sangwan A., Jassal H. K., 2019, *J. Cosmology Astropart. Phys.*, **2019**, 047
- Sinha S., Banerjee N., 2021, *J. Cosmology Astropart. Phys.*, **2021**, 060
- Solà Peracaula J., de Cruz Pérez J., Gómez-Valent A., 2018, *MNRAS*, **478**, 4357
- Solà Peracaula J., Gómez-Valent A., de Cruz Pérez J., 2019, *Physics of the Dark Universe*, **25**, 100311
- Tanvir N. R., et al., 2009, *Nature*, **461**, 1254
- Ureña-López L. A., Roy N., 2020, *Phys. Rev. D*, **102**, 063510
- Vagnozzi S., Di Valentino E., Gariazzo S., Melchiorri A., Mena O., Silk J., 2021a, *Physics of the Dark Universe*, **33**, 100851
- Vagnozzi S., Loeb A., Moresco M., 2021b, *ApJ*, **908**, 84
- Velasquez-Toribio A. M., Fabris J. C., 2020, *European Physical Journal C*, **80**, 1210
- Wang F. Y., Dai Z. G., Liang E. W., 2015, *New Astron. Rev.*, **67**, 1
- Wang J. S., Wang F. Y., Cheng K. S., Dai Z. G., 2016, *A&A*, **585**, A68
- Wang F. Y., Hu J. P., Zhang G. Q., Dai Z. G., 2021, preprint, ([arXiv:2106.14155](#))
- Wei J.-J., 2018, *ApJ*, **868**, 29
- Xu T., Chen Y., Xu L., Cao S., 2021, preprint, ([arXiv:2109.02453](#))
- Yang T., Banerjee A., Ó Colgáin E., 2020, *Phys. Rev. D*, **102**, 123532
- Yu H., Ratra B., Wang F.-Y., 2018, *ApJ*, **856**, 3
- Zhai Z., Blanton M., Slosar A., Tinker J., 2017, *ApJ*, **850**, 183
- Zhao D., Xia J.-Q., 2021, *European Physical Journal C*, **81**, 694
- Zheng X., Cao S., Biesiada M., Li X., Liu T., Liu Y., 2021, *Science China Physics, Mechanics, and Astronomy*, **64**, 259511

This paper has been typeset from a *TeX/LaTeX* file prepared by the author.